

# $K^*$ -charmonium dissociation cross sections and charmonium dissociation rates in hadronic matter

Feng-Rong Liu, Shi-Tao Ji, and Xiao-Ming Xu

Department of Physics, Shanghai University, Baoshan, Shanghai 200444, China

## Abstract

$K^*$ -charmonium dissociation reactions in hadronic matter are studied in the Born approximation, in the quark-interchange mechanism, and with a temperature-dependent quark potential. We obtain the temperature dependence of unpolarized cross sections for the reactions:  $K^*J/\psi \rightarrow \bar{D}D_s^+$ ,  $\bar{D}^*D_s^+$ ,  $\bar{D}D_s^{*+}$ , and  $\bar{D}^*D_s^{*+}$ ;  $K^*\psi' \rightarrow \bar{D}D_s^+$ ,  $\bar{D}^*D_s^+$ ,  $\bar{D}D_s^{*+}$ , and  $\bar{D}^*D_s^{*+}$ ;  $K^*\chi_c \rightarrow \bar{D}D_s^+$ ,  $\bar{D}^*D_s^+$ ,  $\bar{D}D_s^{*+}$ , and  $\bar{D}^*D_s^{*+}$ . We use the cross sections for charmonium dissociation in collisions with pion,  $\rho$  meson, kaon, vector kaon, and  $\eta$  meson to calculate dissociation rates of charmonium with the five types of mesons. Because of the temperature dependence of the meson masses, dissociation cross sections, and meson distribution functions, the charmonium dissociation rates generally increase with the increase of temperature and decrease with the increase of charmonium momentum from 2.2 GeV/ $c$ . We find that the first derivative of the dissociation rate with respect to the charmonium momentum is zero when the charmonium is at rest. While the  $\eta + \psi'$  and  $\eta + \chi_c$  dissociation reactions can be neglected, the  $J/\psi$ ,  $\psi'$ , and  $\chi_c$  dissociation are caused by the collisions with pion,  $\rho$  meson, kaon, vector kaon, and  $\eta$  meson.

Keywords: Charmonium dissociation, Quark-interchange mechanism, Dissociation rate.

PACS: 25.75.-q; 24.85.+p; 12.38.Mh

## I. INTRODUCTION

Hadronic matter is produced in relativistic heavy ion collisions at the Relativistic Heavy Ion Collider and at the Large Hadron Collider. Pions in hadronic matter have a number density smaller than a quark-gluon plasma, but the meson species is not limited to the pion and hadronic matter has a lifetime longer than the plasma. Hence, meson-charmonium dissociation reactions may cause appreciable suppression of charmonia in hadronic matter. In order to separate the suppression of charmonia in hadronic matter so that the suppression due to the quark-gluon plasma is identified, we need to study the meson-charmonium dissociation reactions.

Three approaches have been established for the study of charmonium dissociation in collisions with hadrons. In the short-distance approach the operator product expansion of perturbative QCD is applied to heavy quarkonia of small sizes [1, 2]. Cross sections for nucleon- $J/\psi$  and pion- $J/\psi$  dissociation have been obtained in Refs. [1–3] from existing parton distribution functions [4–6]. In the quark-interchange approach the quark interchange mechanism between the incident hadron and the charmonium breaks the charmonium, and produces charmed mesons and/or charmed strange mesons. Charmonia in collisions with  $\pi$ ,  $\rho$ ,  $K$ , and  $N$  have been studied in Refs. [7–10]. In the meson-exchange approach meson exchange between the two initial mesons breaks the charmonium, and effective Lagrangians with meson couplings are constructed to describe the motion of meson fields. The  $J/\psi$  dissociation in collisions with  $\pi$ ,  $\rho$ ,  $\omega$ ,  $K$ ,  $K^*$ ,  $\eta$ , and  $\phi$  has been considered in Refs. [11–17].

The studies in Refs. [1–3, 7–17] concentrate on charmonium dissociation in vacuum. In hadronic matter charmonium dissociation is affected by the medium [18]. We have obtained the energy and temperature dependence of dissociation cross sections of charmonia in collisions with  $\pi$ ,  $\rho$ ,  $K$ , and  $\eta$  mesons in hadronic matter [19, 20]. Charmonium dissociation reactions may be endothermic in one temperature region and exothermic in another. Peak cross sections of endothermic reactions change with temperature. The  $\eta + J/\psi$  dissociation gives rise to  $J/\psi$  suppression comparable to the suppression caused by the  $\pi + J/\psi$  dissociation [20].

The  $K^* + J/\psi$  dissociation in vacuum was considered in the meson-exchange approach

in Ref. [13], but no cross sections were presented. The energy and temperature dependence of  $K^*$ -charmonium dissociation cross sections are unknown. In hadronic matter the quark interaction, meson masses, and mesonic quark-antiquark relative motion depend on temperature. From vacuum to medium the  $K^*$ -charmonium dissociation reactions must change. Therefore, in this work we calculate the dissociation cross sections of  $J/\psi$ ,  $\psi'$ , and  $\chi_c$  in collisions with  $K^*$  in hadronic matter on the basis of the quark-interchange mechanism [21], the Born approximation, and a temperature-dependent quark potential. Furthermore, from the energy and temperature dependence of the cross sections we calculate the dissociation rate of charmonium with vector kaons. Since the dissociation cross sections of charmonia in collisions with  $\pi$ ,  $\rho$ ,  $K$ , and  $\eta$  mesons are provided in Refs. [19,20], we also calculate the dissociation rates of charmonium with pion,  $\rho$  meson, kaon, and  $\eta$  meson. From these dissociation rates we know different contributions to the charmonium dissociation from different mesons in hadronic matter.

This paper is organized as follows. In Sec. II we introduce cross-section formulas, a central spin-independent potential, and a spin-spin interaction. In Sec. III we present numerical unpolarized cross sections for twelve  $K^*$ -charmonium dissociation reactions and relevant discussions. In Sec. IV we define the dissociation rate of charmonium with meson in hadronic matter, calculate the dissociation rates of charmonium with pion,  $\rho$  meson, kaon, vector kaon, and  $\eta$  meson, and discuss relevant results. In Sec. V we summarize the present work.

## II. CROSS-SECTION FORMULAS

Let  $J_i$ ,  $m_i$ , and  $P_i = (E_i, \vec{P}_i)$  be the angular momentum, mass, and four-momentum of meson  $i$  ( $i = q\bar{q}, c\bar{c}, q\bar{c}, c\bar{q}$ ) in the reaction  $q\bar{q} + c\bar{c} \rightarrow q\bar{c} + c\bar{q}$ , respectively.  $q$  stands for the up quark, down quark or strange quark. The flavor of the quark  $q$  may be different from the flavor of the antiquark  $\bar{q}$ . The unpolarized cross section for  $q\bar{q} + c\bar{c} \rightarrow q\bar{c} + c\bar{q}$  is

$$\sigma^{\text{unpol}}(\sqrt{s}, T) = \frac{(2\pi)^4}{4\sqrt{(P_{q\bar{q}} \cdot P_{c\bar{c}})^2 - m_{q\bar{q}}^2 m_{c\bar{c}}^2}} \int \frac{d^3 P_{q\bar{c}}}{(2\pi)^3 2E_{q\bar{c}}} \frac{d^3 P_{c\bar{q}}}{(2\pi)^3 2E_{c\bar{q}}}$$

$$\frac{1}{(2J_{q\bar{q}} + 1)(2J_{c\bar{c}} + 1)} \sum_{J_{q\bar{q}z} J_{c\bar{c}z} J_{q\bar{c}z} J_{c\bar{q}z}} |\mathcal{M}_{\text{fi}}|^2 \delta(E_{\text{f}} - E_{\text{i}}) \delta(\vec{P}_{\text{f}} - \vec{P}_{\text{i}}), \quad (1)$$

where  $s$  is the Mandelstam variable given by  $s = (E_{q\bar{q}} + E_{c\bar{c}})^2 - (\vec{P}_{q\bar{q}} + \vec{P}_{c\bar{c}})^2$ ,  $T$  is the temperature,  $\mathcal{M}_{\text{fi}}$  is the transition amplitude,  $J_{iz}$  is the magnetic projection quantum number of  $J_i$  ( $i = q\bar{q}, c\bar{c}, q\bar{c}, c\bar{q}$ ),  $E_i = E_{q\bar{q}} + E_{c\bar{c}}$ ,  $E_{\text{f}} = E_{q\bar{c}} + E_{c\bar{q}}$ ,  $\vec{P}_{\text{i}} = \vec{P}_{q\bar{q}} + \vec{P}_{c\bar{c}}$ , and  $\vec{P}_{\text{f}} = \vec{P}_{q\bar{c}} + \vec{P}_{c\bar{q}}$ . If the orbital angular momenta of the four mesons are zero, the unpolarized cross section is

$$\sigma^{\text{unpol}}(\sqrt{s}, T) = \frac{(2\pi)^4}{4\sqrt{(P_{q\bar{q}} \cdot P_{c\bar{c}})^2 - m_{q\bar{q}}^2 m_{c\bar{c}}^2}} \int \frac{d^3 P_{q\bar{c}}}{(2\pi)^3 2E_{q\bar{c}}} \frac{d^3 P_{c\bar{q}}}{(2\pi)^3 2E_{c\bar{q}}} \frac{1}{(2S_{q\bar{q}} + 1)(2S_{c\bar{c}} + 1)} \sum_S (2S + 1) |\mathcal{M}_{\text{fi}}|^2 \delta(E_{\text{f}} - E_{\text{i}}) \delta(\vec{P}_{\text{f}} - \vec{P}_{\text{i}}), \quad (2)$$

where  $S_{q\bar{q}}$  and  $S_{c\bar{c}}$  are the spins of  $q\bar{q}$  and  $c\bar{c}$ , respectively, and  $S$  is the total spin of the two initial mesons. If the orbital angular momenta of  $q\bar{q}$ ,  $c\bar{c}$ ,  $q\bar{c}$ , and  $c\bar{q}$  are 0,  $L_{c\bar{c}}$ , 0, and 0, respectively, the unpolarized cross section is

$$\sigma^{\text{unpol}}(\sqrt{s}, T) = \frac{(2\pi)^4}{4\sqrt{(P_{q\bar{q}} \cdot P_{c\bar{c}})^2 - m_{q\bar{q}}^2 m_{c\bar{c}}^2}} \int \frac{d^3 P_{q\bar{c}}}{(2\pi)^3 2E_{q\bar{c}}} \frac{d^3 P_{c\bar{q}}}{(2\pi)^3 2E_{c\bar{q}}} \sum_{JSL_{c\bar{c}z}} (2J + 1)(2S + 1) \left\{ \begin{array}{ccc} 0 & S_{q\bar{q}} & S_{q\bar{q}} \\ L_{c\bar{c}} & S_{c\bar{c}} & J_{c\bar{c}} \\ L_{c\bar{c}} & S & J \end{array} \right\}^2 |\mathcal{M}_{\text{fi}}|^2 \delta(E_{\text{f}} - E_{\text{i}}) \delta(\vec{P}_{\text{f}} - \vec{P}_{\text{i}}), \quad (3)$$

where the braces give the  $9j$  coefficient,  $J$  is the total angular momentum of the two initial mesons, and  $L_{c\bar{c}z}$  is the magnetic projection quantum number of  $L_{c\bar{c}}$ . Furthermore, if  $L_{c\bar{c}} = 1$  and  $S_{c\bar{c}} = 0$  or  $1$ , the unpolarized cross section is

$$\sigma^{\text{unpol}}(\sqrt{s}, T) = \frac{(2\pi)^4}{4\sqrt{(P_{q\bar{q}} \cdot P_{c\bar{c}})^2 - m_{q\bar{q}}^2 m_{c\bar{c}}^2}} \int \frac{d^3 P_{q\bar{c}}}{(2\pi)^3 2E_{q\bar{c}}} \frac{d^3 P_{c\bar{q}}}{(2\pi)^3 2E_{c\bar{q}}} \frac{1}{(2S_{q\bar{q}} + 1)(2S_{c\bar{c}} + 1)(2L_{c\bar{c}} + 1)} \sum_{SL_{c\bar{c}z}} (2S + 1) |\mathcal{M}_{\text{fi}}|^2 \delta(E_{\text{f}} - E_{\text{i}}) \delta(\vec{P}_{\text{f}} - \vec{P}_{\text{i}}). \quad (4)$$

Define

$$\sigma(S, m_S, \sqrt{s}, T) = \frac{(2\pi)^4}{4\sqrt{(P_{q\bar{q}} \cdot P_{c\bar{c}})^2 - m_{q\bar{q}}^2 m_{c\bar{c}}^2}}$$

$$\int \frac{d^3 P_{q\bar{c}}}{(2\pi)^3 2E_{q\bar{c}}} \frac{d^3 P_{c\bar{q}}}{(2\pi)^3 2E_{c\bar{q}}} |\mathcal{M}_{\text{fi}}|^2 \delta(E_f - E_i) \delta(\vec{P}_f - \vec{P}_i), \quad (5)$$

where  $m_S$  is the magnetic projection quantum number of  $S$ . Then, Eqs. (2) and (4) are written as

$$\sigma^{\text{unpol}}(\sqrt{s}, T) = \frac{1}{(2S_{q\bar{q}} + 1)(2S_{c\bar{c}} + 1)(2L_{c\bar{c}} + 1)} \sum_{SL_{c\bar{c}z}} (2S + 1) \sigma(S, m_S, \sqrt{s}, T). \quad (6)$$

In the center-of-mass frame of  $q\bar{q}$  and  $c\bar{c}$  [22],

$$\sigma(S, m_S, \sqrt{s}, T) = \frac{1}{32\pi s} \frac{|\vec{P}'(\sqrt{s})|}{|\vec{P}(\sqrt{s})|} \int_0^\pi d\theta |\mathcal{M}_{\text{fi}}|^2 \sin \theta, \quad (7)$$

where  $\vec{P}_{q\bar{q}} = \vec{P}$ ,  $\vec{P}_{q\bar{c}} = \vec{P}'$ , and  $\theta$  is the angle between  $\vec{P}$  and  $\vec{P}'$ . Either the quark interchange between  $q\bar{q}$  and  $c\bar{c}$  or the antiquark interchange leads to the reaction  $q\bar{q} + c\bar{c} \rightarrow q\bar{c} + c\bar{q}$ . In addition to the interchange, an interaction takes place between the quark or the antiquark of meson  $q\bar{q}$  ( $q\bar{c}$ ) and the quark or the antiquark of meson  $c\bar{c}$  ( $c\bar{q}$ ). Diagrams for the reaction are shown in Fig. 1 for the prior form and Fig. 2 for the post form [20]. The scattering in the prior form means that gluon exchange occurs before quark interchange. The corresponding transition amplitude is

$$\mathcal{M}_{\text{fi}}^{\text{prior}} = 4\sqrt{E_{q\bar{q}}E_{c\bar{c}}E_{q\bar{c}}E_{c\bar{q}}} \langle \psi_{q\bar{c}} | \langle \psi_{c\bar{q}} | (V_{q\bar{c}} + V_{c\bar{q}} + V_{qc} + V_{\bar{q}\bar{c}}) | \psi_{q\bar{q}} \rangle | \psi_{c\bar{c}} \rangle, \quad (8)$$

where  $\psi_{q\bar{q}}$  ( $\psi_{c\bar{c}}$ ,  $\psi_{q\bar{c}}$ ,  $\psi_{c\bar{q}}$ ) represents the product of color, spin, flavor, and relative-motion wave functions of  $q\bar{q}$  ( $c\bar{c}$ ,  $q\bar{c}$ ,  $c\bar{q}$ ), and  $V_{q\bar{c}}$  ( $V_{c\bar{q}}$ ,  $V_{qc}$ ,  $V_{\bar{q}\bar{c}}$ ) is the potential of  $q$  and  $\bar{c}$  ( $c$  and  $\bar{q}$ ,  $q$  and  $c$ ,  $\bar{q}$  and  $\bar{c}$ ). From the transition amplitude in the prior form we get

$$\sigma^{\text{prior}}(S, m_S, \sqrt{s}, T) = \frac{1}{32\pi s} \frac{|\vec{P}'(\sqrt{s})|}{|\vec{P}(\sqrt{s})|} \int_0^\pi d\theta |\mathcal{M}_{\text{fi}}^{\text{prior}}|^2 \sin \theta. \quad (9)$$

The scattering in the post form means that gluon exchange occurs after quark interchange. The corresponding transition amplitude is

$$\mathcal{M}_{\text{fi}}^{\text{post}} = 4\sqrt{E_{q\bar{q}}E_{c\bar{c}}E_{q\bar{c}}E_{c\bar{q}}} \langle \psi_{q\bar{c}} | \langle \psi_{c\bar{q}} | (V_{q\bar{q}} + V_{c\bar{c}} + V_{qc} + V_{\bar{q}\bar{c}}) | \psi_{q\bar{q}} \rangle | \psi_{c\bar{c}} \rangle, \quad (10)$$

which gives

$$\sigma^{\text{post}}(S, m_S, \sqrt{s}, T) = \frac{1}{32\pi s} \frac{|\vec{P}'(\sqrt{s})|}{|\vec{P}(\sqrt{s})|} \int_0^\pi d\theta |\mathcal{M}_{\text{fi}}^{\text{post}}|^2 \sin \theta. \quad (11)$$

Since  $\sigma^{\text{prior}}$  may differ from  $\sigma^{\text{post}}$  [23–25], the unpolarized cross section is

$$\sigma^{\text{unpol}}(\sqrt{s}, T) = \frac{1}{(2S_{q\bar{q}} + 1)(2S_{c\bar{c}} + 1)(2L_{c\bar{c}} + 1)} \sum_{SL_{c\bar{c}z}} (2S + 1) \times \frac{\sigma^{\text{prior}}(S, m_S, \sqrt{s}, T) + \sigma^{\text{post}}(S, m_S, \sqrt{s}, T)}{2}. \quad (12)$$

The potential used in Eqs. (8) and (10) includes a central spin-independent potential denoted by  $V_{\text{si}}$  and a spin-spin interaction denoted by  $V_{\text{ss}}$ :

$$V_{ab}(\vec{r}) = V_{\text{si}}(\vec{r}) + V_{\text{ss}}(\vec{r}), \quad (13)$$

where  $ab$  represents  $q\bar{c}$ ,  $c\bar{q}$ ,  $qc$ ,  $\bar{q}\bar{c}$ ,  $q\bar{q}$ , or  $c\bar{c}$ , and  $\vec{r}$  is the relative coordinate of  $a$  and  $b$ . The central spin-independent potential is

$$V_{\text{si}}(\vec{r}) = -\frac{\vec{\lambda}_a}{2} \cdot \frac{\vec{\lambda}_b}{2} \frac{3}{4} D \left[ 1.3 - \left( \frac{T}{T_c} \right)^4 \right] \tanh(Ar) + \frac{\vec{\lambda}_a}{2} \cdot \frac{\vec{\lambda}_b}{2} \frac{6\pi}{25} \frac{v(\lambda r)}{r} \exp(-Er), \quad (14)$$

where  $D = 0.7$  GeV,  $T_c = 0.175$  GeV,  $A = 1.5[0.75 + 0.25(T/T_c)^{10}]^6$  GeV,  $E = 0.6$  GeV,  $\lambda = \sqrt{25/16\pi^2\alpha'}$  with  $\alpha' = 1.04$  GeV<sup>-2</sup>, and  $\vec{\lambda}_a$  are the Gell-Mann matrices for the color generators of constituent  $a$ . The dimensionless function  $v(x)$  [26] is

$$v(x) = \frac{100}{3\pi} \int_0^\infty \frac{dQ}{Q} \left[ \rho(\vec{Q}^2) - \frac{K}{\vec{Q}^2} \right] \sin\left(\frac{Q}{\lambda}x\right), \quad (15)$$

where  $K = 3/16\pi^2\alpha'$  and  $\rho(\vec{Q}^2)$  is the physical running coupling constant at the gluon momentum  $\vec{Q}$ . At short distances the quark interaction is described by perturbative QCD in vacuum, and the expression  $\frac{\vec{\lambda}_a}{2} \cdot \frac{\vec{\lambda}_b}{2} \frac{6\pi}{25} \frac{v(\lambda r)}{r}$  in the second term of Eq. (14) is given by one-gluon exchange plus perturbative one- and two-loop corrections [26]. Lattice QCD calculations have provided numerical quark-antiquark free energies at intermediate and large distances [27]. The potential  $V_{\text{si}}(\vec{r})$  well fits  $\frac{\vec{\lambda}_a}{2} \cdot \frac{\vec{\lambda}_b}{2} \frac{6\pi}{25} \frac{v(\lambda r)}{r}$  at short distances and the free energies at  $T/T_c > 0.55$ .

The spin-spin interaction arises from perturbative one-gluon exchange plus one- and two-loop corrections [28], and includes relativistic effects [9, 21, 29]:

$$V_{\text{ss}}(\vec{r}) = -\frac{\vec{\lambda}_a}{2} \cdot \frac{\vec{\lambda}_b}{2} \frac{16\pi^2}{25} \frac{d^3}{\pi^{3/2}} \exp(-d^2r^2) \frac{\vec{s}_a \cdot \vec{s}_b}{m_a m_b} + \frac{\vec{\lambda}_a}{2} \cdot \frac{\vec{\lambda}_b}{2} \frac{4\pi}{25} \frac{1}{r} \frac{d^2 v(\lambda r)}{dr^2} \frac{\vec{s}_a \cdot \vec{s}_b}{m_a m_b}, \quad (16)$$

where  $\vec{s}_a$  and  $m_a$  are the spin and mass of constituent  $a$ , respectively, and the quantity  $d$  is given by

$$d^2 = \sigma_0^2 \left[ \frac{1}{2} + \frac{1}{2} \left( \frac{4m_a m_b}{(m_a + m_b)^2} \right)^4 \right] + \sigma_1^2 \left( \frac{2m_a m_b}{m_a + m_b} \right)^2, \quad (17)$$

where  $\sigma_0 = 0.15$  GeV and  $\sigma_1 = 0.705$ .

In Eqs. (8) and (10) the colour part of the state  $|\psi_{q\bar{q}}\rangle$  is the familiar colour-singlet state,

$$|q\bar{q}, \text{colour}\rangle = \frac{1}{\sqrt{3}} \sum_{n=1}^3 \sum_{\bar{n}=1}^3 \delta_{n\bar{n}} |n\bar{n}\rangle, \quad (18)$$

where  $n$  and  $\bar{n}$  denote the quark colour and the antiquark colour, respectively. The spin part of  $|\psi_{q\bar{q}}\rangle$  is

$$|S_{q\bar{q}} S_{q\bar{q}z}\rangle = \sum_{S_{qz}} \sum_{S_{\bar{q}z}} \langle \frac{1}{2} \frac{1}{2} S_{qz} S_{\bar{q}z} | S_{q\bar{q}} S_{q\bar{q}z} \rangle | \frac{1}{2} S_{qz} \rangle | \frac{1}{2} S_{\bar{q}z} \rangle, \quad (19)$$

where  $S_{q\bar{q}z}$  is the magnetic projection quantum number of  $S_{q\bar{q}}$ ,  $\langle \frac{1}{2} \frac{1}{2} S_{qz} S_{\bar{q}z} | S_{q\bar{q}} S_{q\bar{q}z} \rangle$  are the Clebsch-Gordan coefficients,  $| \frac{1}{2} S_{qz} \rangle$  is the spin- $\frac{1}{2}$  state with the  $z$  component  $S_{qz}$ , and  $| \frac{1}{2} S_{\bar{q}z} \rangle$  is the spin- $\frac{1}{2}$  state with the  $z$  component  $S_{\bar{q}z}$ . Denote the flavour part of  $|\psi_{q\bar{q}}\rangle$  by  $|q\bar{q}, \text{flavour}\rangle$ , and the flavour wave functions of mesons in the ground-state pseudoscalar nonet and the ground-state vector nonet can be found in Refs. [30, 31]. For instance,  $|q\bar{q}, \text{flavour}\rangle$  is  $|u\bar{s}\rangle$  for  $K^{*+}$ ,  $|d\bar{s}\rangle$  for  $K^{*0}$ ,  $-|s\bar{d}\rangle$  for  $\bar{K}^{*0}$ , or  $|s\bar{u}\rangle$  for  $K^{*-}$ . We calculate the transition amplitudes,  $\mathcal{M}_{\text{fi}}^{\text{prior}}$  and  $\mathcal{M}_{\text{fi}}^{\text{post}}$ , in momentum space, and thus need the relative-motion wave function of  $q\bar{q}$  in momentum space. The relative-motion wave function is denoted by  $\phi_{q\bar{q}\text{rel}}$  and is the product of the spherical harmonics and the Fourier transform of the radial wave function obtained from the Schrödinger equation with the potential given in Eq. (13).  $\phi_{q\bar{q}\text{rel}}$  is normalized according to  $\int \frac{d^3 p_{q\bar{q}}}{(2\pi)^3} \phi_{q\bar{q}\text{rel}}^* \phi_{q\bar{q}\text{rel}} = 1$ , where  $\vec{p}_{q\bar{q}}$  is the relative momentum of  $q$  and  $\bar{q}$ . As the product of the colour, spin, flavour, and relative-motion wave functions of  $q\bar{q}$ ,  $|\psi_{q\bar{q}}\rangle$  is written as

$$|\psi_{q\bar{q}}\rangle = \phi_{q\bar{q}\text{rel}} |q\bar{q}, \text{colour}\rangle |q\bar{q}, \text{flavour}\rangle |S_{q\bar{q}} S_{q\bar{q}z}\rangle. \quad (20)$$

The other wave functions ( $|\psi_{c\bar{c}}\rangle$ ,  $|\psi_{q\bar{c}}\rangle$ , and  $|\psi_{c\bar{q}}\rangle$ ) used in Eqs. (8) and (10) are written similarly as

$$|\psi_{c\bar{c}}\rangle = \phi_{c\bar{c}\text{rel}} |c\bar{c}, \text{colour}\rangle |c\bar{c}, \text{flavour}\rangle |S_{c\bar{c}} S_{c\bar{c}z}\rangle, \quad (21)$$

$$| \psi_{q\bar{c}} \rangle = \phi_{q\bar{c}\text{rel}} | q\bar{c}, \text{colour} \rangle | q\bar{c}, \text{flavour} \rangle | S_{q\bar{c}} S_{q\bar{c}z} \rangle, \quad (22)$$

$$| \psi_{c\bar{q}} \rangle = \phi_{c\bar{q}\text{rel}} | c\bar{q}, \text{colour} \rangle | c\bar{q}, \text{flavour} \rangle | S_{c\bar{q}} S_{c\bar{q}z} \rangle, \quad (23)$$

where  $\phi_{c\bar{c}\text{rel}}$  ( $\phi_{q\bar{c}\text{rel}}$ ,  $\phi_{c\bar{q}\text{rel}}$ ),  $| c\bar{c}, \text{colour} \rangle$  ( $| q\bar{c}, \text{colour} \rangle$ ,  $| c\bar{q}, \text{colour} \rangle$ ),  $| c\bar{c}, \text{flavour} \rangle$  ( $| q\bar{c}, \text{flavour} \rangle$ ,  $| c\bar{q}, \text{flavour} \rangle$ ), and  $| S_{c\bar{c}} S_{c\bar{c}z} \rangle$  ( $| S_{q\bar{c}} S_{q\bar{c}z} \rangle$ ,  $| S_{c\bar{q}} S_{c\bar{q}z} \rangle$ ) are the relative-motion, colour, flavour, and spin parts of  $c\bar{c}$  ( $q\bar{c}$ ,  $c\bar{q}$ ), respectively.

In the prior form of the reaction  $A(q\bar{q}) + B(c\bar{c}) \rightarrow C(q\bar{c}) + D(c\bar{q})$  the colour interaction between a constituent of meson  $A(q\bar{q})$  and a constituent of meson  $B(c\bar{c})$  turns the colour-singlet states  $A$  and  $B$  into colour-octet states of  $q\bar{q}$  and  $c\bar{c}$ , respectively. During propagation of quarks and antiquarks quark interchange, i.e., exchange of  $q$  and  $c$  or of  $\bar{q}$  and  $\bar{c}$  causes  $q$  ( $c$ ) to find  $\bar{c}$  ( $\bar{q}$ ) to get the colour-singlet state  $C$  ( $D$ ). In the post form of  $A(q\bar{q}) + B(c\bar{c}) \rightarrow C(q\bar{c}) + D(c\bar{q})$  quark interchange, i.e., exchange of a constituent of meson  $A$  and a constituent of meson  $B$  produces a colour-octet state of  $q\bar{c}$  and another colour-octet state of  $c\bar{q}$ . The colour interaction between a constituent of  $q\bar{c}$  and a constituent of  $c\bar{q}$  makes  $q\bar{c}$  ( $c\bar{q}$ ) colourless so that the bound state  $C$  ( $D$ ) is formed.

The first term given in Eq. (14) stands for the confining potential. In the confinement regime the mesonic quark-antiquark relative-motion wave functions mainly determined by the confining potential are nonperturbative. At low energies near threshold of  $A(q\bar{q}) + B(c\bar{c}) \rightarrow C(q\bar{c}) + D(c\bar{q})$  the nonperturbative part of the  $q\bar{q}$  and  $c\bar{c}$  wave functions must overlap during the transition from mesons  $A$  and  $B$  to the colour-octet states of  $q\bar{q}$  and  $c\bar{c}$ . Even though the distance of  $q$  and  $\bar{c}$  ( $c$  and  $\bar{q}$ ) is large, the nonperturbative correlation corresponding to the nonperturbative part leads to formation of a bound state of  $q$  and  $\bar{c}$  ( $c$  and  $\bar{q}$ ) [7, 32] during the hadronization of  $q$ ,  $\bar{q}$ ,  $c$ , and  $\bar{c}$  to form mesons  $C$  and  $D$ .

The Schrödinger equation with the potential given in Eq. (13) at  $T = 0$  is solved to reproduce the experimental masses of  $\pi$ ,  $\rho$ ,  $K$ ,  $K^*$ ,  $J/\psi$ ,  $\psi'$ ,  $\chi_c$ ,  $D$ ,  $D^*$ ,  $D_s$ , and  $D_s^*$  mesons [33]. In the Schrödinger equation and the potential the masses of the up quark, the down quark, the strange quark, and the charm quark are 0.32 GeV, 0.32 GeV, 0.5 GeV, and 1.51 GeV, respectively. With the pionic quark-antiquark relative-motion wave functions obtained in solving the Schrödinger equation, the experimental data of  $S$ -wave

$I = 2$  elastic phase shifts for  $\pi\pi$  scattering in vacuum for  $0 < \sqrt{s} < 2.4$  GeV [34–37] are reproduced in the Born approximation and in the quark-interchange mechanism.

### III. NUMERICAL CROSS SECTIONS AND DISCUSSIONS

We establish the notation  $K = \begin{pmatrix} K^+ \\ K^0 \end{pmatrix}$ ,  $\bar{K} = \begin{pmatrix} \bar{K}^0 \\ K^- \end{pmatrix}$ ,  $K^* = \begin{pmatrix} K^{*+} \\ K^{*0} \end{pmatrix}$ ,  $\bar{K}^* = \begin{pmatrix} \bar{K}^{*0} \\ K^{*-} \end{pmatrix}$ ,  $D = \begin{pmatrix} D^+ \\ D^0 \end{pmatrix}$ ,  $\bar{D} = \begin{pmatrix} \bar{D}^0 \\ D^- \end{pmatrix}$ ,  $D^* = \begin{pmatrix} D^{*+} \\ D^{*0} \end{pmatrix}$ , and  $\bar{D}^* = \begin{pmatrix} \bar{D}^{*0} \\ D^{*-} \end{pmatrix}$ . We consider the following reactions:

$$\begin{aligned} K^* + J/\psi &\rightarrow \bar{D} + D_s^+, & K^* + J/\psi &\rightarrow \bar{D}^* + D_s^+, \\ K^* + J/\psi &\rightarrow \bar{D} + D_s^{*+}, & K^* + J/\psi &\rightarrow \bar{D}^* + D_s^{*+}; \\ K^* + \psi' &\rightarrow \bar{D} + D_s^+, & K^* + \psi' &\rightarrow \bar{D}^* + D_s^+, \\ K^* + \psi' &\rightarrow \bar{D} + D_s^{*+}, & K^* + \psi' &\rightarrow \bar{D}^* + D_s^{*+}; \\ K^* + \chi_c &\rightarrow \bar{D} + D_s^+, & K^* + \chi_c &\rightarrow \bar{D}^* + D_s^+, \\ K^* + \chi_c &\rightarrow \bar{D} + D_s^{*+}, & K^* + \chi_c &\rightarrow \bar{D}^* + D_s^{*+}. \end{aligned}$$

These reactions are governed by quark interchange.

The transition amplitudes given in Eqs. (8) and (10) are further written as

$$\begin{aligned} \mathcal{M}_{\text{fi}}^{\text{prior}} &= 4\sqrt{E_{q\bar{q}}E_{c\bar{c}}E_{q\bar{c}}E_{c\bar{q}}} \langle q\bar{c}, \text{flavour} | \langle c\bar{q}, \text{flavour} | q\bar{q}, \text{flavour} \rangle | c\bar{c}, \text{flavour} \rangle \\ &\langle q\bar{c}, \text{colour} | \langle c\bar{q}, \text{colour} | \langle S_{q\bar{c}}S_{q\bar{c}z} | \langle S_{c\bar{q}}S_{c\bar{q}z} | \int \frac{d^3p_{q\bar{c}}}{(2\pi)^3} \frac{d^3p_{c\bar{q}}}{(2\pi)^3} \\ &[\phi_{q\bar{c}\text{rel}}^*(\vec{p}_{q\bar{c}})\phi_{c\bar{q}\text{rel}}^*(\vec{p}_{c\bar{q}})V_{q\bar{c}}\phi_{q\bar{q}\text{rel}}(\vec{p}_{c\bar{q}} + \frac{m_{\bar{q}}}{m_q + m_{\bar{q}}}\vec{P} + \frac{m_{\bar{q}}}{m_c + m_{\bar{q}}}\vec{P}') \\ &\phi_{c\bar{c}\text{rel}}(\vec{p}_{c\bar{q}} + \frac{m_c}{m_c + m_{\bar{c}}}\vec{P} - \frac{m_c}{m_c + m_{\bar{q}}}\vec{P}') \\ &+ \phi_{q\bar{c}\text{rel}}^*(\vec{p}_{q\bar{c}})\phi_{c\bar{q}\text{rel}}^*(\vec{p}_{c\bar{q}})V_{c\bar{q}}\phi_{q\bar{q}\text{rel}}(\vec{p}_{q\bar{c}} - \frac{m_q}{m_q + m_{\bar{q}}}\vec{P} + \frac{m_q}{m_q + m_{\bar{c}}}\vec{P}') \\ &\phi_{c\bar{c}\text{rel}}(\vec{p}_{q\bar{c}} - \frac{m_{\bar{c}}}{m_c + m_{\bar{c}}}\vec{P} - \frac{m_{\bar{c}}}{m_q + m_{\bar{c}}}\vec{P}') \\ &+ \phi_{q\bar{c}\text{rel}}^*(\vec{p}_{q\bar{c}})\phi_{c\bar{q}\text{rel}}^*(\vec{p}_{c\bar{q}})V_{q\bar{c}}\phi_{q\bar{q}\text{rel}}(\vec{p}_{c\bar{q}} + \frac{m_{\bar{q}}}{m_q + m_{\bar{q}}}\vec{P} + \frac{m_{\bar{q}}}{m_c + m_{\bar{q}}}\vec{P}') \\ &\phi_{c\bar{c}\text{rel}}(\vec{p}_{q\bar{c}} - \frac{m_{\bar{c}}}{m_c + m_{\bar{c}}}\vec{P} - \frac{m_{\bar{c}}}{m_q + m_{\bar{c}}}\vec{P}') \\ &+ \phi_{q\bar{c}\text{rel}}^*(\vec{p}_{q\bar{c}})\phi_{c\bar{q}\text{rel}}^*(\vec{p}_{c\bar{q}})V_{q\bar{c}}\phi_{q\bar{q}\text{rel}}(\vec{p}_{q\bar{c}} - \frac{m_q}{m_q + m_{\bar{q}}}\vec{P} + \frac{m_q}{m_q + m_{\bar{c}}}\vec{P}')] \end{aligned}$$

$$\begin{aligned}
& \phi_{c\bar{c}\text{rel}}(\vec{p}_{c\bar{q}} + \frac{m_c}{m_c + m_{\bar{c}}}\vec{P} - \frac{m_c}{m_c + m_{\bar{q}}}\vec{P}') \\
& | S_{q\bar{q}}S_{q\bar{q}z} \rangle | S_{c\bar{c}}S_{c\bar{c}z} \rangle | q\bar{q}, \text{colour} \rangle | c\bar{c}, \text{colour} \rangle,
\end{aligned} \tag{24}$$

$$\begin{aligned}
\mathcal{M}_{\text{fi}}^{\text{post}} &= 4\sqrt{E_{q\bar{q}}E_{c\bar{c}}E_{q\bar{c}}E_{c\bar{q}}} \langle q\bar{c}, \text{flavour} | \langle c\bar{q}, \text{flavour} | q\bar{q}, \text{flavour} \rangle | c\bar{c}, \text{flavour} \rangle \\
& \langle q\bar{c}, \text{colour} | \langle c\bar{q}, \text{colour} | \langle S_{q\bar{c}}S_{q\bar{c}z} | \langle S_{c\bar{q}}S_{c\bar{q}z} | \int \frac{d^3p_{q\bar{q}}}{(2\pi)^3} \frac{d^3p_{c\bar{c}}}{(2\pi)^3} \\
& [\phi_{q\bar{c}\text{rel}}^*(\vec{p}_{c\bar{c}} + \frac{m_{\bar{c}}}{m_c + m_{\bar{c}}}\vec{P} + \frac{m_{\bar{c}}}{m_q + m_{\bar{c}}}\vec{P}') \phi_{c\bar{q}\text{rel}}^*(\vec{p}_{c\bar{c}} - \frac{m_c}{m_c + m_{\bar{c}}}\vec{P} + \frac{m_c}{m_c + m_{\bar{q}}}\vec{P}') \\
& V_{q\bar{q}}\phi_{q\bar{q}\text{rel}}(\vec{p}_{q\bar{q}})\phi_{c\bar{c}\text{rel}}(\vec{p}_{c\bar{c}}) \\
& + \phi_{q\bar{c}\text{rel}}^*(\vec{p}_{q\bar{q}} + \frac{m_q}{m_q + m_{\bar{q}}}\vec{P} - \frac{m_q}{m_q + m_{\bar{c}}}\vec{P}') \phi_{c\bar{q}\text{rel}}^*(\vec{p}_{q\bar{q}} - \frac{m_{\bar{q}}}{m_q + m_{\bar{q}}}\vec{P} - \frac{m_{\bar{q}}}{m_c + m_{\bar{q}}}\vec{P}') \\
& V_{c\bar{c}}\phi_{q\bar{q}\text{rel}}(\vec{p}_{q\bar{q}})\phi_{c\bar{c}\text{rel}}(\vec{p}_{c\bar{c}}) \\
& + \phi_{q\bar{c}\text{rel}}^*(\vec{p}_{c\bar{c}} + \frac{m_{\bar{c}}}{m_c + m_{\bar{c}}}\vec{P} + \frac{m_{\bar{c}}}{m_q + m_{\bar{c}}}\vec{P}') \phi_{c\bar{q}\text{rel}}^*(\vec{p}_{q\bar{q}} - \frac{m_{\bar{q}}}{m_q + m_{\bar{q}}}\vec{P} - \frac{m_{\bar{q}}}{m_c + m_{\bar{q}}}\vec{P}') \\
& V_{qc}\phi_{q\bar{q}\text{rel}}(\vec{p}_{q\bar{q}})\phi_{c\bar{c}\text{rel}}(\vec{p}_{c\bar{c}}) \\
& + \phi_{q\bar{c}\text{rel}}^*(\vec{p}_{q\bar{q}} + \frac{m_q}{m_q + m_{\bar{q}}}\vec{P} - \frac{m_q}{m_q + m_{\bar{c}}}\vec{P}') \phi_{c\bar{q}\text{rel}}^*(\vec{p}_{c\bar{c}} - \frac{m_c}{m_c + m_{\bar{c}}}\vec{P} + \frac{m_c}{m_c + m_{\bar{q}}}\vec{P}') \\
& V_{\bar{q}\bar{c}}\phi_{q\bar{q}\text{rel}}(\vec{p}_{q\bar{q}})\phi_{c\bar{c}\text{rel}}(\vec{p}_{c\bar{c}})] \\
& | S_{q\bar{q}}S_{q\bar{q}z} \rangle | S_{c\bar{c}}S_{c\bar{c}z} \rangle | q\bar{q}, \text{colour} \rangle | c\bar{c}, \text{colour} \rangle,
\end{aligned} \tag{25}$$

where  $\vec{p}_{c\bar{c}}$  ( $\vec{p}_{q\bar{c}}$ ,  $\vec{p}_{c\bar{q}}$ ) is the relative momentum of  $c$  and  $\bar{c}$  ( $q$  and  $\bar{c}$ ,  $c$  and  $\bar{q}$ ). Given the wave functions in Eqs. (20)-(23), we calculate colour matrix elements, flavour matrix elements, spin matrix elements, and spatial matrix elements. The colour matrix elements  $\langle q\bar{c}, \text{colour} | \langle c\bar{q}, \text{colour} | \frac{\vec{\lambda}_a}{2} \cdot \frac{\vec{\lambda}_b}{2} | q\bar{q}, \text{colour} \rangle | c\bar{c}, \text{colour} \rangle$  are  $-4/9$  for  $V_{q\bar{c}}$ ,  $V_{c\bar{q}}$ ,  $V_{q\bar{q}}$ , and  $V_{c\bar{c}}$  and  $4/9$  for  $V_{qc}$  and  $V_{\bar{q}\bar{c}}$ . For antiquarks  $\frac{\vec{\lambda}_a}{2}$  ( $\frac{\vec{\lambda}_b}{2}$ ) is as usual replaced by  $-\frac{\vec{\lambda}_a^T}{2}$  ( $-\frac{\vec{\lambda}_b^T}{2}$ ). For the twelve  $K^*$ -charmonium dissociation reactions the flavour matrix elements  $\langle q\bar{c}, \text{flavour} | \langle c\bar{q}, \text{flavour} | q\bar{q}, \text{flavour} \rangle | c\bar{c}, \text{flavour} \rangle$  equal 1. Since the spin operator  $\vec{s}_q + \vec{s}_{\bar{q}} + \vec{s}_c + \vec{s}_{\bar{c}}$  commutes with the potential  $V_{ab}$ , the total spin of the two initial mesons equals the total spin of the two final mesons. The spin matrix elements  $\langle S_{q\bar{c}}S_{q\bar{c}z} | \langle S_{c\bar{q}}S_{c\bar{q}z} | \vec{s}_a \cdot \vec{s}_b | S_{q\bar{q}}S_{q\bar{q}z} \rangle | S_{c\bar{c}}S_{c\bar{c}z} \rangle$  are independent of the magnetic projection quantum number  $m_S$ , and depend on the total spin and the spins of the four

mesons. The values of the spin matrix elements can be found in Ref. [21].

The spatial matrix elements are expressed as the two integrals in Eqs. (24) and (25). The two integrals involve the quark-antiquark relative-motion wave functions. Diagrams “C1 prior” and “C2 prior” in Fig. 1 are “capture” diagrams [21] because the interacting quark-antiquark pair scatter into the same final meson. Diagrams “C1 post” and “C2 post” in Fig. 2 are also “capture” diagrams because the interacting quark-antiquark pair come from the same initial meson. The interacting quark-antiquark pair are in the colour-singlet state, so are the other quark-antiquark pair. Diagrams “T1 prior”, “T2 prior”, “T1 post”, and “T2 post” are “transfer” diagrams [21] because the interacting quark-quark or antiquark-antiquark pair scatter (transfer momentum) into different final mesons in the prior form or come (bring momentum) from different initial mesons in the post form. The mesonic quark-antiquark relative-motion wave functions are functions of the quark-antiquark relative momenta. The interaction between two constituents and the quark interchange result in that the quark-antiquark relative momenta are related between an initial meson and a final meson through the linear combination of  $\vec{P}$  and  $\vec{P}'$ . For example, from the first term enclosed by brackets in  $\mathcal{M}_{\text{fi}}^{\text{prior}}$  we get  $\vec{p}_{q\bar{q}} = \vec{p}_{c\bar{q}} + \frac{m_{\bar{q}}}{m_q+m_{\bar{q}}}\vec{P} + \frac{m_{\bar{q}}}{m_c+m_{\bar{q}}}\vec{P}'$  and  $\vec{p}_{c\bar{c}} = \vec{p}_{c\bar{q}} + \frac{m_c}{m_c+m_{\bar{c}}}\vec{P} - \frac{m_c}{m_c+m_{\bar{q}}}\vec{P}'$ , and from the third term enclosed by brackets in  $\mathcal{M}_{\text{fi}}^{\text{post}}$  we get  $\vec{p}_{q\bar{c}} = \vec{p}_{c\bar{c}} + \frac{m_{\bar{c}}}{m_c+m_{\bar{c}}}\vec{P} + \frac{m_{\bar{c}}}{m_q+m_{\bar{c}}}\vec{P}'$  and  $\vec{p}_{c\bar{q}} = \vec{p}_{q\bar{q}} - \frac{m_{\bar{q}}}{m_q+m_{\bar{q}}}\vec{P} - \frac{m_{\bar{q}}}{m_c+m_{\bar{q}}}\vec{P}'$ . For “capture” diagrams and “transfer” diagrams the relation is different. Corresponding to the “capture” diagrams “C1 prior” and “C2 prior”, the quark-antiquark relative momenta of the two initial mesons are only related to the quark-antiquark relative momentum of the final meson which is not the interacting quark-antiquark pair. Corresponding to the “capture” diagrams “C1 post” and “C2 post”, the quark-antiquark relative momenta of the two final mesons are only related to the quark-antiquark relative momentum of the initial meson which is not the interacting quark-antiquark pair. As to the “transfer” diagrams the quark-antiquark relative momentum of a final meson (another final meson) is only related to the one of an initial meson (another initial meson). In low-energy meson-meson collisions  $|\vec{P}|$  and  $|\vec{P}'|$  are small. This allows small values for  $|\vec{p}_{q\bar{q}}|$  and  $|\vec{p}_{c\bar{c}}|$  as seen from  $\mathcal{M}_{\text{fi}}^{\text{prior}}$  and  $|\vec{p}_{q\bar{c}}|$  and  $|\vec{p}_{c\bar{q}}|$  as seen from  $\mathcal{M}_{\text{fi}}^{\text{post}}$ .  $\phi_{q\bar{q}\text{rel}}(\vec{p}_{q\bar{q}})$  ( $\phi_{c\bar{c}\text{rel}}(\vec{p}_{c\bar{c}})$ ),

$\phi_{q\bar{c}\text{rel}}(\vec{p}_{q\bar{c}})$ ,  $\phi_{c\bar{q}\text{rel}}(\vec{p}_{c\bar{q}})$ ) decreases rapidly while  $|\vec{p}_{q\bar{q}}|$  ( $|\vec{p}_{c\bar{c}}|$ ,  $|\vec{p}_{q\bar{c}}|$ ,  $|\vec{p}_{c\bar{q}}|$ ) increases. Then, the nonperturbative part of the mesonic quark-antiquark relative-motion wave functions makes dominant contributions to  $\mathcal{M}_{\text{fi}}^{\text{prior}}$  and  $\mathcal{M}_{\text{fi}}^{\text{post}}$ . In high-energy meson-meson collisions  $|\vec{P}|$  and  $|\vec{P}'|$  are large. The absolute values of  $\vec{p}_{q\bar{q}}$  and  $\vec{p}_{c\bar{c}}$  in  $\mathcal{M}_{\text{fi}}^{\text{prior}}$  and of  $\vec{p}_{q\bar{c}}$  and  $\vec{p}_{c\bar{q}}$  in  $\mathcal{M}_{\text{fi}}^{\text{post}}$  are generally large. The perturbative part of the mesonic quark-antiquark relative-motion wave functions, which is mainly determined by the second term in Eq. (14) and the spin-spin interaction, significantly affects  $\mathcal{M}_{\text{fi}}^{\text{prior}}$  and  $\mathcal{M}_{\text{fi}}^{\text{post}}$ .

According to Eq. (12) we calculate unpolarized cross sections at the six temperatures  $T/T_c = 0, 0.65, 0.75, 0.85, 0.9, \text{ and } 0.95$ . In Figs. 3-14 we plot the unpolarized cross sections for the twelve  $K^*$ -charmonium dissociation reactions. Depending on temperature, a reaction is either endothermic or exothermic. The numerical cross sections for endothermic reactions are parametrized as

$$\begin{aligned} \sigma^{\text{unpol}}(\sqrt{s}, T) = & a_1 \left( \frac{\sqrt{s} - \sqrt{s_0}}{b_1} \right)^{c_1} \exp \left[ c_1 \left( 1 - \frac{\sqrt{s} - \sqrt{s_0}}{b_1} \right) \right] \\ & + a_2 \left( \frac{\sqrt{s} - \sqrt{s_0}}{b_2} \right)^{c_2} \exp \left[ c_2 \left( 1 - \frac{\sqrt{s} - \sqrt{s_0}}{b_2} \right) \right], \end{aligned} \quad (26)$$

where  $\sqrt{s_0}$  is the threshold energy, and  $a_1$ ,  $b_1$ ,  $c_1$ ,  $a_2$ ,  $b_2$ , and  $c_2$  are parameters. The numerical cross sections for exothermic reactions are parametrized as

$$\begin{aligned} \sigma^{\text{unpol}}(\sqrt{s}, T) = & \frac{\vec{P}'^2}{\vec{P}^2} \left\{ a_1 \left( \frac{\sqrt{s} - \sqrt{s_0}}{b_1} \right)^{c_1} \exp \left[ c_1 \left( 1 - \frac{\sqrt{s} - \sqrt{s_0}}{b_1} \right) \right] \right. \\ & \left. + a_2 \left( \frac{\sqrt{s} - \sqrt{s_0}}{b_2} \right)^{c_2} \exp \left[ c_2 \left( 1 - \frac{\sqrt{s} - \sqrt{s_0}}{b_2} \right) \right] \right\}. \end{aligned} \quad (27)$$

The parameter values are listed in Tables 1-3. We follow a procedure presented in Ref. [19] to get cross sections at any temperature between  $0.65T_c$  and  $T_c$ . This needs the quantities  $d_0$  and  $\sqrt{s_z}$  which are also listed in Tables 1-3.  $d_0$  is the separation between the peak's location on the  $\sqrt{s}$ -axis and the threshold energy, and  $\sqrt{s_z}$  is the square root of the Mandelstam variable at which the cross section is 1/100 of the peak cross section.

The cross sections for the three  $K^* + J/\psi$  reactions in Figs. 4-6 show that the peak cross section of each reaction decreases when temperature changes from  $T/T_c = 0.65$  to 0.85 and increases when temperature changes from  $T/T_c = 0.85$  to 0.95. While temperature

increases, the value of the central spin-independent potential at large distances becomes smaller and smaller (the confinement becomes weaker and weaker), and the Schrödinger equation produces increasing meson radii. Decrease in peak cross section is caused by weakening confinement. Increase in peak cross section is caused by increasing radii of initial mesons. When the decrease is faster than the increase, the peak cross section of each reaction shown in Figs. 4-6 goes down as temperature changes from  $0.65T_c$  to  $0.85T_c$ . When the decrease is slower than the increase, the peak cross section of each reaction goes up as temperature changes from  $0.85T_c$  to  $0.95T_c$ .

As shown by Fig. 1 of Ref. [19], the  $\psi'$  mass is very close to the  $\chi_c$  mass for  $0.6T_c \leq T < T_c$ . While temperature increases, the sum of the initial-meson masses decreases more rapidly than the sum of the final-meson masses. Any  $K^* + \psi'$  reaction shown in Figs. 7-10 is endothermic above a temperature and exothermic below the temperature. The  $K^* + \chi_c$  reaction that has the same final states as the  $K^* + \psi'$  reaction is endothermic above or exothermic below almost the same temperature. However, since the  $\chi_c$  and  $\psi'$  mesons have different quantum numbers, the cross section for the  $K^* + \chi_c$  reaction is not identical to the one for the  $K^* + \psi'$  reaction.

The  $K^*$  meson and the  $K$  meson have the same strangeness, and the difference of the  $K^*$  mass ( $m_{K^*}$ ) and the  $K$  mass ( $m_K$ ) becomes smaller and smaller with increasing temperature. Since the experimental mass splitting  $m_{K^*} - m_K = 0.3963$  GeV is large, the largest cross section of an exothermic  $K^* + \text{charmonium}$  reaction shown by the curve at  $T = 0$  is larger than the one of the exothermic  $K + \text{charmonium}$  reaction with the same final states [20]. At  $T \rightarrow T_c$  the  $K^*$  and  $K$  mesons become degenerate in mass. As shown by the curves at  $T/T_c = 0.95$ , all the  $K^* + \text{charmonium}$  reactions become endothermic. The largest cross sections of the four reactions,  $K^* + \psi' \rightarrow \bar{D} + D_s^{*+}$ ,  $K^* + \chi_c \rightarrow \bar{D}^* + D_s^+$ ,  $K^* + \chi_c \rightarrow \bar{D} + D_s^{*+}$ , and  $K^* + \chi_c \rightarrow \bar{D}^* + D_s^{*+}$ , become smaller than the ones of the four reactions,  $K + \psi' \rightarrow \bar{D} + D_s^{*+}$ ,  $K + \chi_c \rightarrow \bar{D}^* + D_s^+$ ,  $K + \chi_c \rightarrow \bar{D} + D_s^{*+}$ , and  $K + \chi_c \rightarrow \bar{D}^* + D_s^{*+}$ , respectively. This is owed to the difference in the mesonic space wave function, in the spin matrix element of the spin-spin interaction, and in the overlap of the initial and final spin wave functions related to the central spin-independent potential.

The  $\bar{K}^*$ -charmonium dissociation includes

$$\begin{aligned}
&\bar{K}^* + J/\psi \rightarrow D_s^- + D, \quad \bar{K}^* + J/\psi \rightarrow D_s^{*-} + D, \\
&\bar{K}^* + J/\psi \rightarrow D_s^- + D^*, \quad \bar{K}^* + J/\psi \rightarrow D_s^{*-} + D^*; \\
&\bar{K}^* + \psi' \rightarrow D_s^- + D, \quad \bar{K}^* + \psi' \rightarrow D_s^{*-} + D, \\
&\bar{K}^* + \psi' \rightarrow D_s^- + D^*, \quad \bar{K}^* + \psi' \rightarrow D_s^{*-} + D^*; \\
&\bar{K}^* + \chi_c \rightarrow D_s^- + D, \quad \bar{K}^* + \chi_c \rightarrow D_s^{*-} + D, \\
&\bar{K}^* + \chi_c \rightarrow D_s^- + D^*, \quad \bar{K}^* + \chi_c \rightarrow D_s^{*-} + D^*.
\end{aligned}$$

Cross sections for these reactions are obtained from the  $K^*$ -charmonium dissociation reactions. For example, the cross section for  $\bar{K}^* + J/\psi \rightarrow D_s^- + D$  equals the cross section for  $K^* + J/\psi \rightarrow \bar{D} + D_s^+$ .

With the quark potential given in Eq. (13) at  $T = 0$  we can reproduce the experimental masses of  $\pi$ ,  $\rho$ ,  $K$ ,  $K^*$ ,  $J/\psi$ ,  $\psi'$ ,  $\chi_c$ ,  $D$ ,  $D^*$ ,  $D_s$ , and  $D_s^*$  mesons. In the Born approximation and in the quark-interchange mechanism the experimental data of  $S$ -wave  $I = 2$  elastic phase shifts for  $\pi\pi$  scattering in vacuum can be reproduced. Therefore, we calculate  $K^*$ -charmonium dissociation cross sections with the quark potential, in the Born approximation and in the quark-interchange mechanism. The study of meson-charmonium dissociation reactions is itself of theoretical interest. Unfortunately, no direct meson-charmonium collision experiments are possible. Up to now, attempts to constrain theoretical models about  $\pi J/\psi \rightarrow \pi\psi'$  have been made in Refs. [38–40] from the experimental data on the hadronic decay  $\psi' \rightarrow \pi\pi J/\psi$ . We can not use the cross sections obtained in Refs. [38–40] for  $\pi J/\psi \rightarrow \pi\psi'$  to constrain our charmonium dissociation cross sections since the reaction can not be studied in the quark-interchange mechanism. However, we can use the experimental data on elastic  $\pi\pi$  scattering for  $I = 2$  and elastic  $\pi K$  scattering for  $I = 3/2$  to examine our cross sections for  $\pi J/\psi$ ,  $\pi\chi_c$ , and  $\pi\psi'$  dissociation. This is because the five types of reactions are governed by the quark-interchange mechanism and have the pion as an incident hadron. The comparison of our theoretical results with the experimental data is shown in Fig. 30. The solid, dashed, and dotted curves indicate the cross sections obtained in Ref. [19] for  $\pi J/\psi \rightarrow \bar{D}^*D + \bar{D}D^* + \bar{D}^*D^*$ ,

for  $\pi\psi' \rightarrow \bar{D}^*D + \bar{D}D^* + \bar{D}^*D^*$ , and for  $\pi\chi_c \rightarrow \bar{D}^*D + \bar{D}D^* + \bar{D}^*D^*$ , respectively. The experimental data were obtained in the region  $\sqrt{s} < 2.8$  GeV, and the theoretical results are given in the region  $\sqrt{s} \geq 3.87583$  GeV. The two regions are different. To make an easy comparison, the three curves have been translated by -3 GeV in  $\sqrt{s}$ . Solving the Schrödinger equation with the potential given in Eq. (13) at  $T = 0$ , we obtain 0.45, 0.534, 0.595, 0.672, and 0.757 fm as the radii of  $J/\psi$ ,  $\pi$ ,  $K$ ,  $\chi_c$ , and  $\psi'$  mesons, respectively. The larger the radii of initial mesons, the larger the cross section for a reaction. The spin-spin interaction is proportional to the inverse of the product of the masses of two interacting constituents. From the elastic  $\pi\pi$  scattering or the elastic  $\pi K$  scattering to the  $\pi$ -charmonium dissociation reactions, at least one quark mass changes from the up-quark or strange-quark mass to the charm-quark mass. Correspondingly, the contribution of the spin-spin interaction to the cross section gets appreciably smaller. Therefore, the peak cross section of  $\pi J/\psi$  dissociation is much smaller than the experimental data on the elastic  $\pi K$  scattering for  $I = 3/2$ . Even though the  $\chi_c$  radius is by 13% larger than the  $K$  radius, the peak cross section of the  $\pi\chi_c$  dissociation is smaller than the largest experimental datum of the elastic  $\pi K$  scattering. Since the  $\psi'$  radius is largest among the radii of  $J/\psi$ ,  $\pi$ ,  $K$ ,  $\chi_c$ , and  $\psi'$  mesons, the peak cross section of the  $\pi\psi'$  dissociation is close to the experimental data on the elastic  $\pi\pi$  scattering for  $I = 2$  given in Ref. [41]. Hence, the peak cross sections of the  $\pi$ -charmonium dissociation have reasonable orders of magnitude. We can thus expect that other meson-charmonium dissociation has reasonable orders of magnitude of peak cross sections.

An indirect way to examine meson-charmonium dissociation cross sections, which has been suggested in references, e.g. Ref. [13], is to use the cross sections to calculate nuclear modification factor of  $J/\psi$  produced in relativistic heavy-ion collisions. The collisions may produce charmonia and hadronic matter simultaneously, and the charmonia may break up travelling through hadronic matter. If the cross sections are unreasonably large, the charmonia dissociated by hadronic matter cause  $J/\psi$  suppression stronger than observed suppression. The measured nuclear modification factor of  $J/\psi$  thus places a constraint on the charmonium dissociation cross sections. In a future study we will calculate the

nuclear modification factor using our charmonium dissociation cross sections.

## IV. DISSOCIATION RATES AND DISCUSSIONS

In hadronic matter random motion of a kind of hadrons leads to a momentum distribution. We use the meson distribution function and the unpolarized cross section to define the dissociation rate of charmonium in the interaction with meson. The unpolarized cross sections obtained with the quark potential, in the quark-interchange mechanism, and in the Born approximation are used to calculate the dissociation rates in hadronic matter.

### A. Dissociation rate

Cross sections for  $\pi$ -charmonium dissociation reactions and  $\rho$ -charmonium dissociation reactions were obtained in Ref. [19], and cross sections for  $K$ -charmonium dissociation reactions,  $\bar{K}$ -charmonium dissociation reactions, and  $\eta$ -charmonium dissociation reactions were obtained in Ref. [20]. In hadronic matter the meson distribution is given by

$$f_i(\vec{k}) = \frac{1}{e^{\sqrt{k^2+m_i^2}/T} - 1}, \quad (28)$$

where  $m_i$  and  $\vec{k}$  are the mass and momentum of the meson, respectively. The number density of meson species  $i$  is

$$n_i = g_i \int \frac{d^3k}{(2\pi)^3} f_i(\vec{k}), \quad (29)$$

where  $g_i$  is the spin-isospin degeneracy factor, and equals 3 for  $\pi$ , 9 for  $\rho$ , 4 for  $K$  and  $\bar{K}$ , 12 for  $K^*$  and  $\bar{K}^*$ , and 1 for  $\eta$ , respectively. The thermal-averaged meson-charmonium dissociation cross section is

$$\langle v_{\text{rel}} \sigma^{\text{unpol}}(\sqrt{s}, T) \rangle = \frac{g_i \int \frac{d^3k}{(2\pi)^3} v_{\text{rel}} \sigma^{\text{unpol}}(\sqrt{s}, T) f_i(\vec{k})}{g_i \int \frac{d^3k}{(2\pi)^3} f_i(\vec{k})}, \quad (30)$$

where  $v_{\text{rel}}$  is the relative velocity of the meson and the charmonium. Since  $v_{\text{rel}}$  relies on the meson and charmonium masses, it depends on temperature. The dissociation rate of charmonium in the interaction with meson species  $i$  in hadronic matter is

$$n_i \langle v_{\text{rel}} \sigma^{\text{unpol}}(\sqrt{s}, T) \rangle = \frac{g_i}{4\pi^2} \int_0^\infty \int_0^\pi d|\vec{k}| d\theta \sin \theta \vec{k}^2 v_{\text{rel}} \sigma^{\text{unpol}}(\sqrt{s}, T) f_i(\vec{k}), \quad (31)$$

where  $\theta$  is the angle between the meson momentum and the charmonium momentum and which determines the charmonium suppression due to meson-charmonium dissociation in hadronic matter. Since the meson distribution, the unpolarized cross section, and the relative velocity vary with temperature, the dissociation rate depends on temperature. The dissociation rate of  $J/\psi$  with  $\pi$  is obtained while  $\sigma^{\text{unpol}}$  is the sum of the cross sections for  $\pi + J/\psi \rightarrow \bar{D}^* + D$ ,  $\pi + J/\psi \rightarrow \bar{D} + D^*$ , and  $\pi + J/\psi \rightarrow \bar{D}^* + D^*$ . The dissociation rate of  $\psi'$  with vector kaon is obtained while  $\sigma^{\text{unpol}}$  is the sum of the cross sections for  $K^* + \psi' \rightarrow \bar{D} + D_s^+$ ,  $K^* + \psi' \rightarrow \bar{D}^* + D_s^+$ ,  $K^* + \psi' \rightarrow \bar{D} + D_s^{*+}$ , and  $K^* + \psi' \rightarrow \bar{D}^* + D_s^{*+}$ . Other dissociation rates for charmonium with meson can be similarly calculated according to Table 4.

## B. Numerical results and discussions

We calculate dissociation rates of charmonium with pion,  $\rho$  meson, kaon, vector kaon, and  $\eta$  meson in hadronic matter. Numerical results of the rates as functions of charmonium momentum are plotted in Figs. 15-29. The dissociation rates of charmonium with pion,  $\rho$  meson, kaon, vector kaon, and  $\eta$  meson are shown by the dashed curves, the dotted curves, the dot-dashed curves, the dot-dash-dashed curves, and the dot-dot-dashed curves, respectively. In Figs. 15-19 (Figs. 20-24, Figs. 25-29) every solid curve stands for the  $J/\psi$  ( $\psi'$ ,  $\chi_c$ ) dissociation rate, and is the sum of the dissociation rates of  $J/\psi$  ( $\psi'$ ,  $\chi_c$ ) with pion,  $\rho$  meson, kaon, vector kaon, and  $\eta$  meson. While temperature increases, the charmonium dissociation rates increase except the  $\chi_c$  dissociation rate at  $T/T_c = 0.9$ . This indicates that the higher the temperature is, the stronger charmonium suppression the mesons cause. Excluding the  $J/\psi$  dissociation rate at  $T/T_c = 0.65$  and  $0.75$ , the dissociation rates decrease while the charmonium momentum increases. At  $T/T_c = 0.65$  in Fig. 15 the dissociation rate of  $J/\psi$  with  $\pi$  increases (decreases) when the  $J/\psi$  momentum goes up to (from) 4.7 GeV/ $c$ , and the one of  $J/\psi$  with kaon increases (decreases) when the  $J/\psi$  momentum goes up to (from) 3.3 GeV/ $c$ . Hence, the  $J/\psi$  dissociation rate at  $T/T_c = 0.65$  has a maximum at  $\sqrt{s} = 2.2$  GeV. A similar case at  $T/T_c = 0.75$  is shown in Fig. 16. The decrease of the dissociation rates with the increase of charmonium momentum can

be understood with two situations in the following. While the charmonium momentum increases, the Mandelstam variable  $s$  of meson and charmonium increases,  $\sqrt{s}$  becomes far away from the threshold energy, and the unpolarized cross section decreases. While the charmonium momentum increases, it is also possible that  $\sqrt{s}$  does not become far away from the threshold energy. This corresponds to the nearly collinear motion of meson and charmonium. The angle  $\theta$  in Eq. (31) is thus small, and the contribution to the integration from such  $\vec{k}$  is negligible. The two situations make the dissociation rate decrease while the charmonium momentum increases.

In Eq. (31) the relative velocity is

$$v_{\text{rel}} = \frac{\sqrt{(P_i \cdot P_{c\bar{c}})^2 - m_i^2 m_{c\bar{c}}^2}}{E_i E_{c\bar{c}}}, \quad (32)$$

where the meson four-momentum is  $P_i = (E_i, \vec{k})$  and from which we get

$$\frac{\partial v_{\text{rel}}}{\partial |\vec{P}_{c\bar{c}}|} = \left( \frac{P_i \cdot P_{c\bar{c}}}{v_{\text{rel}} E_i E_{c\bar{c}}} - v_{\text{rel}} \right) \frac{|\vec{P}_{c\bar{c}}|}{E_{c\bar{c}}^2} - \frac{|\vec{k}| |P_i \cdot P_{c\bar{c}}| \cos \theta}{v_{\text{rel}} E_i^2 E_{c\bar{c}}^2}. \quad (33)$$

The unpolarized cross sections are functions of temperature and the Mandelstam variable

$$s = (P_i + P_{c\bar{c}})^2 = m_i^2 + m_{c\bar{c}}^2 + 2P_i \cdot P_{c\bar{c}}, \quad (34)$$

from which we have

$$\frac{\partial \sqrt{s}}{\partial |\vec{P}_{c\bar{c}}|} = \frac{1}{\sqrt{s}} \left( \frac{E_i}{E_{c\bar{c}}} |\vec{P}_{c\bar{c}}| - |\vec{k}| \cos \theta \right). \quad (35)$$

The first derivative of the dissociation rate with respect to the charmonium momentum is

$$\begin{aligned} \frac{\partial n_i \langle v_{\text{rel}} \sigma^{\text{unpol}}(\sqrt{s}, T) \rangle}{\partial |\vec{P}_{c\bar{c}}|} &= \frac{g_i}{4\pi^2} \int_0^\infty \int_0^\pi d|\vec{k}| d\theta \sin \theta \vec{k}^2 \\ &\left( \frac{\partial v_{\text{rel}}}{\partial |\vec{P}_{c\bar{c}}|} \sigma^{\text{unpol}}(\sqrt{s}, T) + v_{\text{rel}} \frac{\partial \sigma^{\text{unpol}}(\sqrt{s}, T)}{\partial \sqrt{s}} \frac{\partial \sqrt{s}}{\partial |\vec{P}_{c\bar{c}}|} \right) f_i(\vec{k}). \end{aligned} \quad (36)$$

When the charmonium momentum is 0, the first derivative is 0. This result is indicated by all curves in Figs. 15-29, and means that the dissociation rate of very slowly moving charmonium equals the dissociation rate of charmonium at rest.

In hadronic matter the pion number density is higher than the number density of any other meson species. Since the pion is lightest among all mesons, the relative velocity of pion and charmonium is larger than the one of any other meson species with the same momentum and the charmonium. Since the dissociation rate is proportional to the relative velocity and the meson distribution function, the dissociation rate of charmonium with  $\pi$  is most concerned, and is a benchmark for determining the importance of the dissociation rate of charmonium with any other meson species.

When the  $J/\psi$  meson is at rest, the dissociation rate of  $J/\psi$  with  $\rho$  ( $K^* + \bar{K}^*$ ,  $K + \bar{K}$ ) is about 4.37 (3.52, 0.76), 1.23 (1.93, 0.86), 1.16 (1.52, 0.94), 1.78 (1.78, 0.97), and 4.98 (1.17, 0.3) times the one of  $J/\psi$  with  $\pi$  at  $T/T_c = 0.65, 0.75, 0.85, 0.9,$  and  $0.95$ , respectively. The dissociation rate of  $J/\psi$  with  $\rho$  ( $K^* + \bar{K}^*$ ,  $K + \bar{K}$ ) is larger (larger, smaller) than the one of  $J/\psi$  with  $\pi$  at low  $J/\psi$  momenta. At  $T/T_c=0.85$  the dissociation rate of  $J/\psi$  with  $\eta$  is larger than the dissociation rate of  $J/\psi$  with  $\pi$  when the  $J/\psi$  momentum is smaller than 1 GeV/ $c$ . Only at  $T/T_c=0.95$  the dissociation rate of  $J/\psi$  with  $\eta$  is much smaller than the dissociation rate of  $J/\psi$  with  $\pi$ . The  $J/\psi$  dissociation rate at  $T/T_c = 0.95$  is much larger than the one at  $T/T_c = 0.65, 0.75, 0.85,$  and  $0.9$ . For example, the  $J/\psi$  dissociation rate at  $T/T_c = 0.95$  is about 7.94 times the one at  $T/T_c = 0.9$ . This is because that the endothermic  $J/\psi$  dissociation in collisions with pion,  $\rho$  meson, kaon, and vector kaon takes a rapid rise in peak cross sections when temperature approaches the critical temperature.

The dissociation rate of  $\psi'$  with  $\rho$  is smaller than the one of  $\psi'$  with  $\pi$  at  $T/T_c = 0.65$  and  $0.75$ , and larger than the one of  $\psi'$  with  $\pi$  at  $T/T_c = 0.85, 0.9,$  and  $0.95$  when the  $\psi'$  momentum is smaller than 3.3 GeV/ $c$ . At  $T/T_c = 0.85$  the dissociation rate of  $\psi'$  with vector kaon is larger than the one of  $\psi'$  with  $\pi$  when the  $\psi'$  momentum is smaller than 2.6 GeV/ $c$ . The dissociation rate of  $\psi'$  with vector kaon is smaller than the one of  $\psi'$  with  $\pi$  at  $T/T_c = 0.9$  and  $0.95$ , and is very small at  $T/T_c = 0.65$  and  $0.75$ . At any temperature in this region  $0.6 \leq T/T_c < 1$ , the dissociation rate of  $\psi'$  with kaon is smaller than the one of  $\psi'$  with pion. The dissociation rate of  $\psi'$  with  $\eta$  is very small, and the  $\eta + \psi'$  reactions can be neglected.

The dissociation rate of  $\chi_c$  with  $\rho$  is smaller than the one of  $\chi_c$  with  $\pi$  at  $T/T_c = 0.65$ ,  $0.75$ , and  $0.95$ , and larger than the one of  $\chi_c$  with  $\pi$  at  $T/T_c = 0.85$  and  $0.9$  when the  $\chi_c$  momentum is smaller than  $4 \text{ GeV}/c$ . The dissociation rate of  $\chi_c$  with vector kaon is much smaller than the one of  $\chi_c$  with  $\pi$  at  $T/T_c = 0.65$  and  $0.75$ . However, at  $T/T_c = 0.85$  and  $0.9$  the dissociation rate of  $\chi_c$  with vector kaon is larger than the one of  $\chi_c$  with  $\pi$  when the  $\chi_c$  momentum is smaller than about  $2 \text{ GeV}/c$ . For  $0.6 \leq T/T_c < 1$  the dissociation rate of  $\chi_c$  with kaon is smaller than the one of  $\chi_c$  with pion. The dissociation rate of  $\chi_c$  with  $\eta$  is quite small, and the  $\eta + \chi_c$  reactions can be neglected.

The vector-kaon mass is larger than the kaon mass, and the vector-kaon distribution function is smaller than the kaon distribution function. When a vector kaon and a kaon have the same momentum, the relative velocity between the vector kaon and a charmonium is smaller than the one between the kaon and the charmonium. However, these do not mean that the dissociation rate of charmonium with vector kaon must be smaller than the dissociation rate of charmonium with kaon. We account for this by the dissociation rates of  $J/\psi$  with vector kaon and of  $J/\psi$  with kaon at  $T/T_c = 0.75$ . The peak cross section of the endothermic reaction  $K^* + J/\psi \rightarrow \bar{D}^* + D_s^+$  is larger than the one of the endothermic reaction  $K + J/\psi \rightarrow \bar{D}^* + D_s^+$ . The peak cross section of  $K^* + J/\psi \rightarrow \bar{D}^* + D_s^{*+}$  is larger than the one of  $K + J/\psi \rightarrow \bar{D}^* + D_s^{*+}$ . Even though the peak cross section of  $K^* + J/\psi \rightarrow \bar{D} + D_s^{*+}$  is smaller than the one of  $K + J/\psi \rightarrow \bar{D} + D_s^{*+}$ , the sum of the peak cross sections of  $K^* + J/\psi \rightarrow \bar{D}^* + D_s^+$ ,  $K^* + J/\psi \rightarrow \bar{D} + D_s^{*+}$ , and  $K^* + J/\psi \rightarrow \bar{D}^* + D_s^{*+}$  is larger than the sum of the peak cross sections of  $K + J/\psi \rightarrow \bar{D}^* + D_s^+$ ,  $K + J/\psi \rightarrow \bar{D} + D_s^{*+}$ , and  $K + J/\psi \rightarrow \bar{D}^* + D_s^{*+}$ . The  $K^*$ -induced  $J/\psi$  dissociation has the exothermic reaction  $K^* + J/\psi \rightarrow \bar{D} + D_s^+$ , but the  $K$ -induced  $J/\psi$  dissociation does not produce the final states,  $\bar{D}$  and  $D_s^+$ . In addition, while  $\sqrt{s}$  increases from the threshold energy, the cross sections for the  $K^* + J/\psi$  dissociation reactions increase more rapidly than the ones for the  $K + J/\psi$  dissociation reactions. Therefore, at  $T/T_c = 0.75$  the dissociation rate of  $J/\psi$  with vector kaon is larger than the one of  $J/\psi$  with kaon when the  $J/\psi$  momentum is smaller than  $2.1 \text{ GeV}/c$ . In the same way we can understand that the dissociation rate of  $\chi_c$  with vector kaon at  $T/T_c = 0.95$  is larger than the one of  $\chi_c$  with kaon even though the

largest cross sections of the three reactions,  $K^* + \chi_c \rightarrow \bar{D}^* + D_s^+$ ,  $K^* + \chi_c \rightarrow \bar{D} + D_s^{*+}$ , and  $K^* + \chi_c \rightarrow \bar{D}^* + D_s^{*+}$ , are smaller than the ones of the three reactions,  $K + \chi_c \rightarrow \bar{D}^* + D_s^+$ ,  $K + \chi_c \rightarrow \bar{D} + D_s^{*+}$ , and  $K + \chi_c \rightarrow \bar{D}^* + D_s^{*+}$ , respectively, as mentioned in Sec. III.

## V. SUMMARY

The unpolarized cross sections for twelve  $K^*$ -charmonium dissociation reactions have been obtained in the quark-interchange mechanism, in the Born approximation and with the quark potential. The temperature dependence of the quark potential, the meson masses, and the mesonic quark-antiquark relative-motion wave functions leads to the temperature dependence of the unpolarized cross sections. Even though  $\psi'$  and  $\chi_c$  have very similar masses, their different quantum numbers cause different cross sections for  $K^* + \psi'$  and  $K^* + \chi_c$  reactions. Even though the  $K^*$  mass is larger than the  $K$  mass, the cross sections for some  $K^*$ -charmonium dissociation reactions may be smaller than the ones for the  $K$ -charmonium dissociation reactions with the same final states at  $T \rightarrow T_c$ .

Using the dissociation cross sections of charmonia in collisions with pion,  $\rho$  meson, kaon, vector kaon, and  $\eta$  meson, we have calculated the dissociation rates of charmonium with pion,  $\rho$  meson, kaon, vector kaon, and  $\eta$  meson. The first derivative of the dissociation rates with respect to the charmonium momentum is zero at zero charmonium momentum. The temperature dependence of the cross section, the relative velocity, and the distribution function brings about the temperature dependence of the dissociation rates. When the temperature increases, charmonium dissociation rates generally increase. With charmonium momentum increasing from 2.2 GeV/ $c$ , the dissociation rates decrease. The dissociation rates of  $J/\psi$  with the five species of mesons are comparable at low  $J/\psi$  momenta, and the five species of mesons contribute to the  $J/\psi$  suppression in hadronic matter. The dissociation rates of  $\psi'$  with  $\rho$  meson and vector kaon are larger than the one of  $\psi'$  with pion in some momentum and temperature regions. To study the  $\psi'$  suppression, the  $\psi'$  dissociation in collisions with pion,  $\rho$  meson, kaon, and vector kaon needs to be considered, but the  $\eta + \psi'$  reactions can be neglected. This also holds true for the  $\chi_c$  case.

## ACKNOWLEDGEMENTS

We thank Prof. H. J. Weber for helpful discussions. This work was supported by the National Natural Science Foundation of China under Grant No. 11175111.

## References

- [1] D. Kharzeev and H. Satz, Phys. Lett. B 334, 155 (1994).
- [2] M. E. Peskin, Nucl. Phys. B 156, 365 (1979); G. Bhanot and M. E. Peskin, Nucl. Phys. B 156, 391 (1979).
- [3] F. Arleo, P. B. Gossiaux, T. Gousset, and J. Aichelin, Phys. Rev. D 65, 014005 (2001).
- [4] H. L. Lai *et al.*, Phys. Rev. D 51, 4763 (1995).
- [5] A. D. Martin, W. J. Stirling, and R. G. Roberts, Phys. Rev. D 50, 6734 (1994); Phys. Rev. D 51, 4756 (1995).
- [6] M. Glück, E. Reya, and A. Vogt, Z. Phys. C 67, 433 (1995); M. Glück, E. Reya, and M. Stratmann, Eur. Phys. J. C 2, 159 (1998); M. Glück, E. Reya, and I. Schienbein, Eur. Phys. J. C 10, 313 (1999).
- [7] K. Martins, D. Blaschke, and E. Quack, Phys. Rev. C 51, 2723 (1995).
- [8] C.-Y. Wong, E. S. Swanson, and T. Barnes, Phys. Rev. C 62, 045201 (2000); Phys. Rev. C 65, 014903 (2001).
- [9] T. Barnes, E. S. Swanson, C.-Y. Wong, and X.-M. Xu, Phys. Rev. C 68, 014903 (2003).
- [10] J. P. Hilbert, N. Black, T. Barnes, and E. S. Swanson, Phys. Rev. C 75, 064907 (2007).

- [11] S. G. Matinyan and B. Müller, Phys. Rev. C 58, 2994 (1998).
- [12] Z. Lin and C.M. Ko, Phys. Rev. C 62, 034903 (2000); J. Phys. G 27, 617 (2001).
- [13] K.L. Haglin, Phys. Rev. C 61, 031902 (2000); K. L. Haglin and C. Gale, Phys. Rev. C 63, 065201 (2001).
- [14] Y. Oh, T. Song, and S. H. Lee, Phys. Rev. C 63, 034901 (2001).
- [15] F. S. Navarra, M. Nielsen, and M. R. Robilotta, Phys. Rev. C 64, 021901(R) (2001).
- [16] L. Maiani, F. Piccinini, A. D. Polosa, and V. Riquer, Nucl. Phys. A 741, 273 (2004).
- [17] A. Bourque and C. Gale, Phys. Rev. C 78, 035206 (2008); Phys. Rev. C 80, 015204 (2009).
- [18] C.-Y. Wong, Phys. Rev. C 65, 034902 (2002).
- [19] J. Zhou and X.-M. Xu, Phys. Rev. C 85, 064904 (2012).
- [20] S.-T. Ji, Z.-Y. Shen, and X.-M. Xu, J. Phys. G 42, 095110 (2015).
- [21] T. Barnes and E. S. Swanson, Phys. Rev. D 46, 131 (1992); E. S. Swanson, Ann. Phys. (N.Y.) 220, 73 (1992).
- [22] Y.-Q. Li and X.-M. Xu, Nucl. Phys. A 794, 210 (2007).
- [23] N. F. Mott and H. S. W. Massey, The Theory of Atomic Collisions, Clarendon Press, Oxford, 1965.
- [24] T. Barnes, N. Black, and E. S. Swanson, Phys. Rev. C 63, 025204 (2001).
- [25] C.-Y. Wong and H. W. Crater, Phys. Rev. C 63, 044907 (2001).
- [26] W. Buchmüller and S.-H. H. Tye, Phys. Rev. D 24, 132 (1981).
- [27] F. Karsch, E. Laermann, and A. Peikert, Nucl. Phys. B 605, 579 (2001).
- [28] X.-M. Xu, Nucl. Phys. A 697, 825 (2002).

- [29] S. Godfrey and N. Isgur, Phys. Rev. D 32, 189 (1985).
- [30] F. E. Close, An Introduction to Quarks and Partons, Academic Press, New York, 1979.
- [31] D. Griffiths, Introduction to Elementary Particles, Harper & Row Publishers, New York, 1987.
- [32] D. Blaschke and G. Röpke, Phys. Lett. B 299, 332 (1993).
- [33] K. Nakamura *et al.*, Particle Data Group, J. Phys. G 37, 075021 (2010).
- [34] E. Colton *et al.*, Phys. Rev. D 3, 2028 (1971).
- [35] N. B. Durusoy *et al.*, Phys. Lett. B 45, 517 (1973).
- [36] W. Hoogland *et al.*, Nucl. Phys. B 126, 109 (1977).
- [37] M. J. Losty *et al.*, Nucl. Phys. B 69, 185 (1974).
- [38] T. Barnes and N. I. Kochelev, J. Phys. G 30, 1811 (2004).
- [39] H. Sorge, E. V. Shuryak, and I. Zahed, Phys. Rev. Lett. 79, 2775 (1997).
- [40] J. W. Chen and M. J. Savage, Phys. Rev. D 57, 2837 (1998).
- [41] D. Cohen, T. Ferbel, P. Slattery, and B. Werner, Phys. Rev. D 7, 661 (1973).
- [42] B. Jongejans *et al.*, Nucl. Phys. B 67, 381 (1973).
- [43] D. Linglin *et al.*, Nucl. Phys. B 57, 64 (1973).

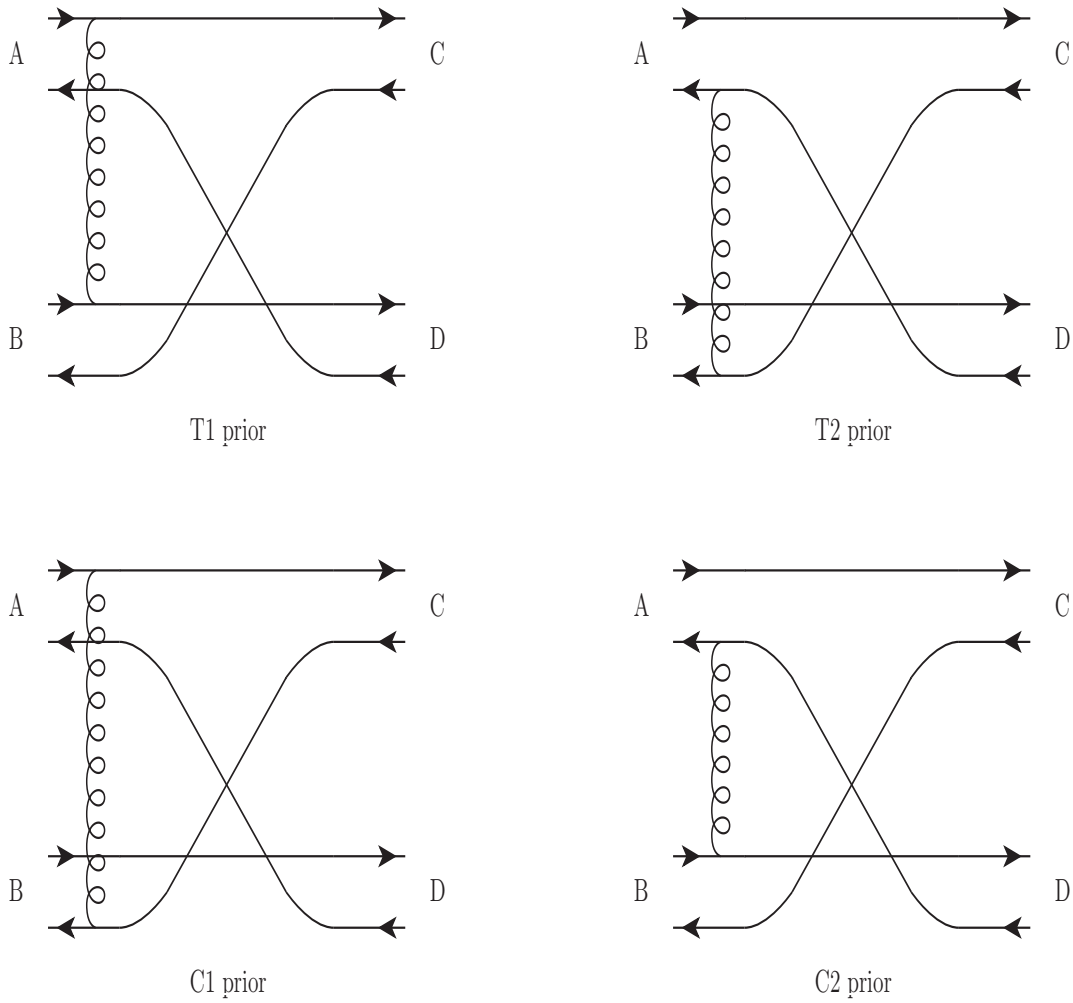


Figure 1: 'Prior' diagrams. Solid (wavy) lines represent quarks or antiquarks (interaction). This figure is reproduced under permission from the article with doi:10.1088/0954-3899/42/9/095110.

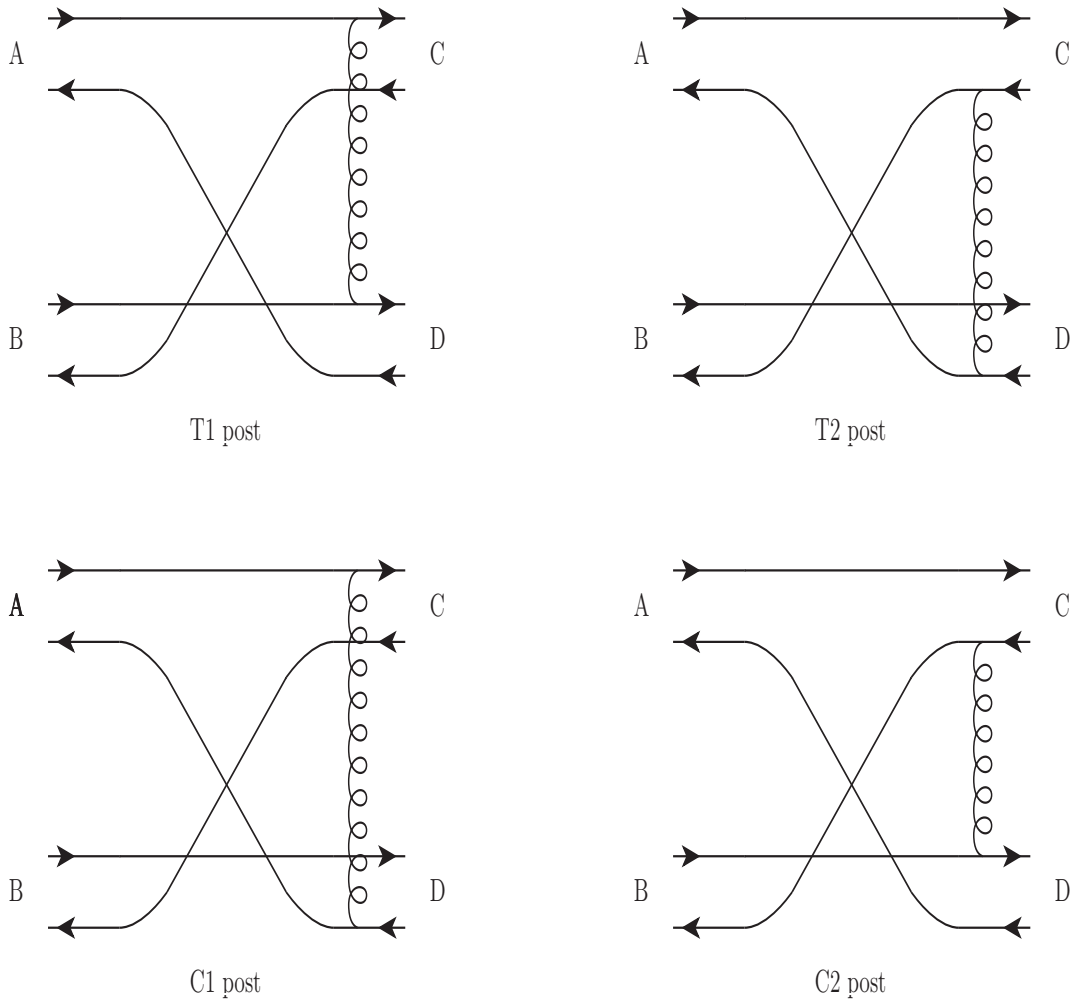


Figure 2: 'Post' diagrams. Solid (wavy) lines represent quarks or antiquarks (interaction). This figure is reproduced under permission from the article with doi:10.1088/0954-3899/42/9/095110.

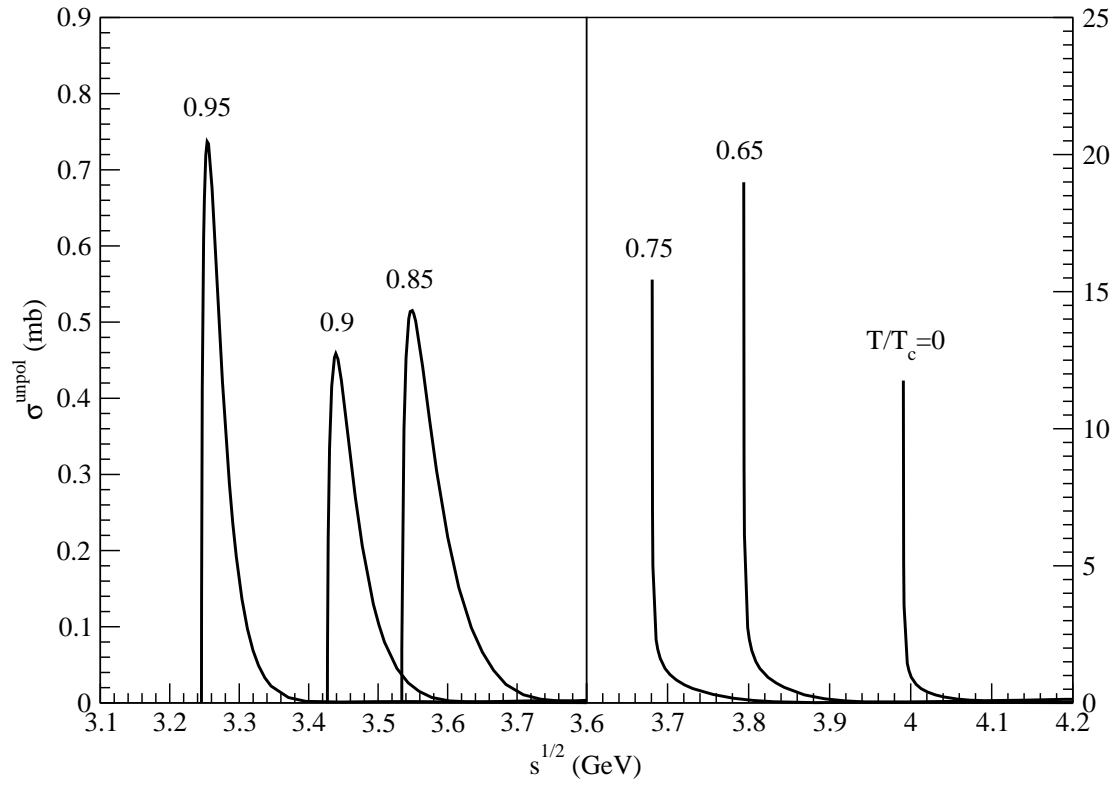


Figure 3: Cross sections for  $K^* + J/\psi \rightarrow \bar{D} + D_s^+$  at various temperatures.

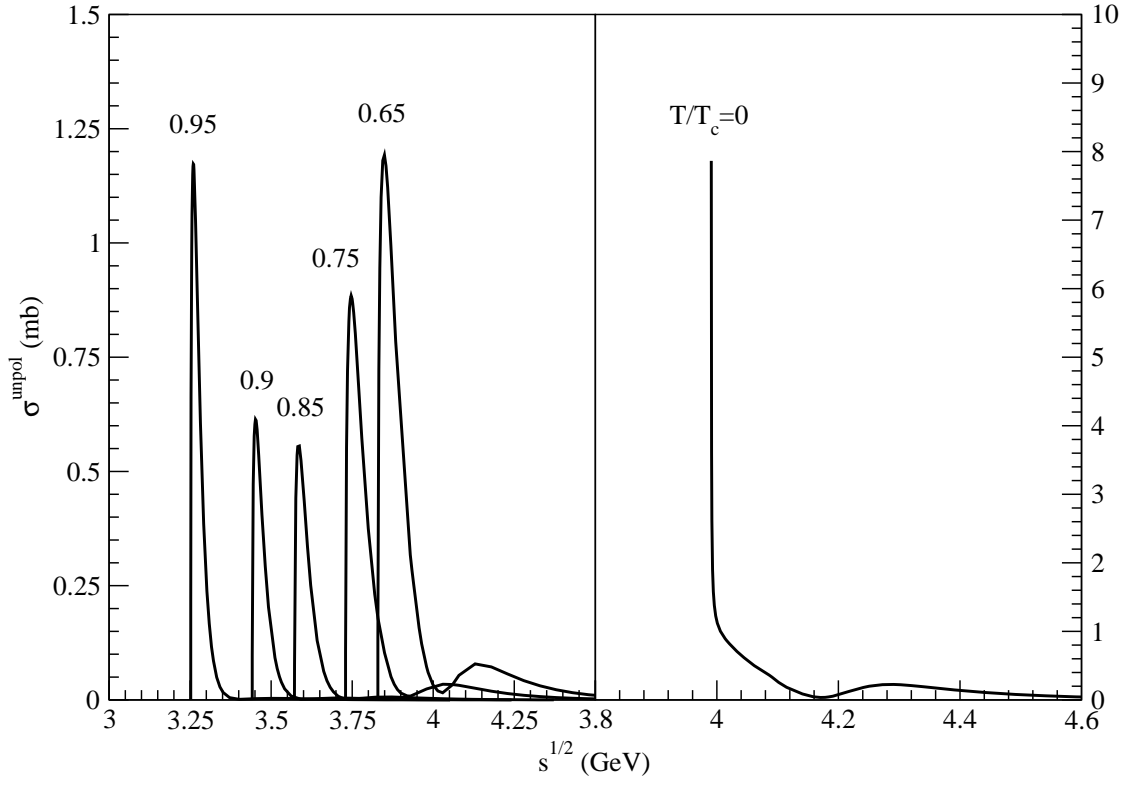


Figure 4: Cross sections for  $K^* + J/\psi \rightarrow \bar{D}^* + D_s^+$  at various temperatures.

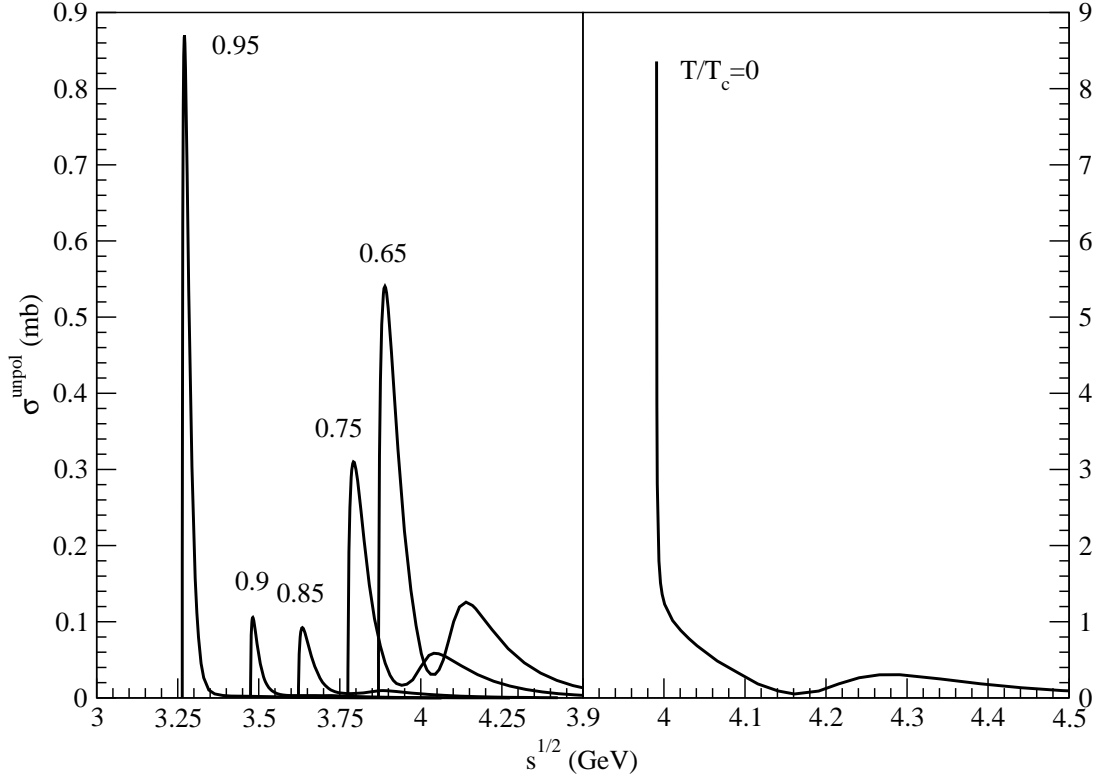


Figure 5: Cross sections for  $K^* + J/\psi \rightarrow \bar{D} + D_s^{*+}$  at various temperatures.

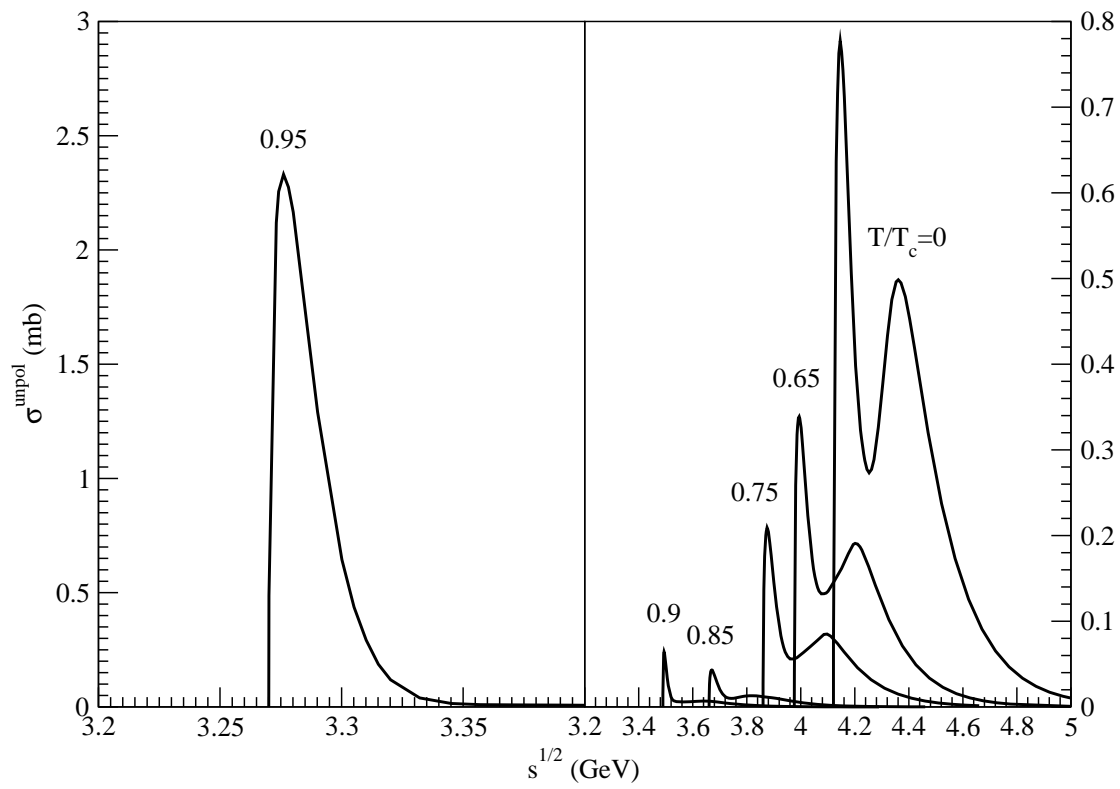


Figure 6: Cross sections for  $K^* + J/\psi \rightarrow \bar{D}^* + D_s^{*+}$  at various temperatures.

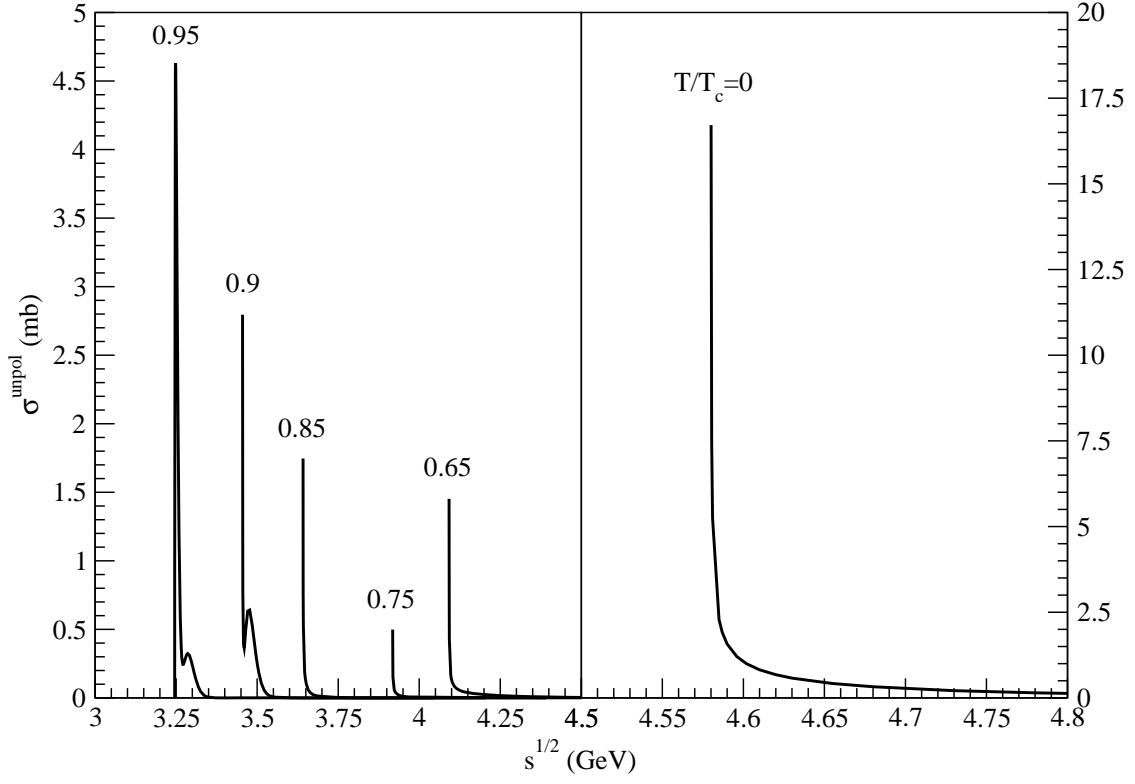


Figure 7: Cross sections for  $K^* + \psi' \rightarrow \bar{D} + D_s^+$  at various temperatures.

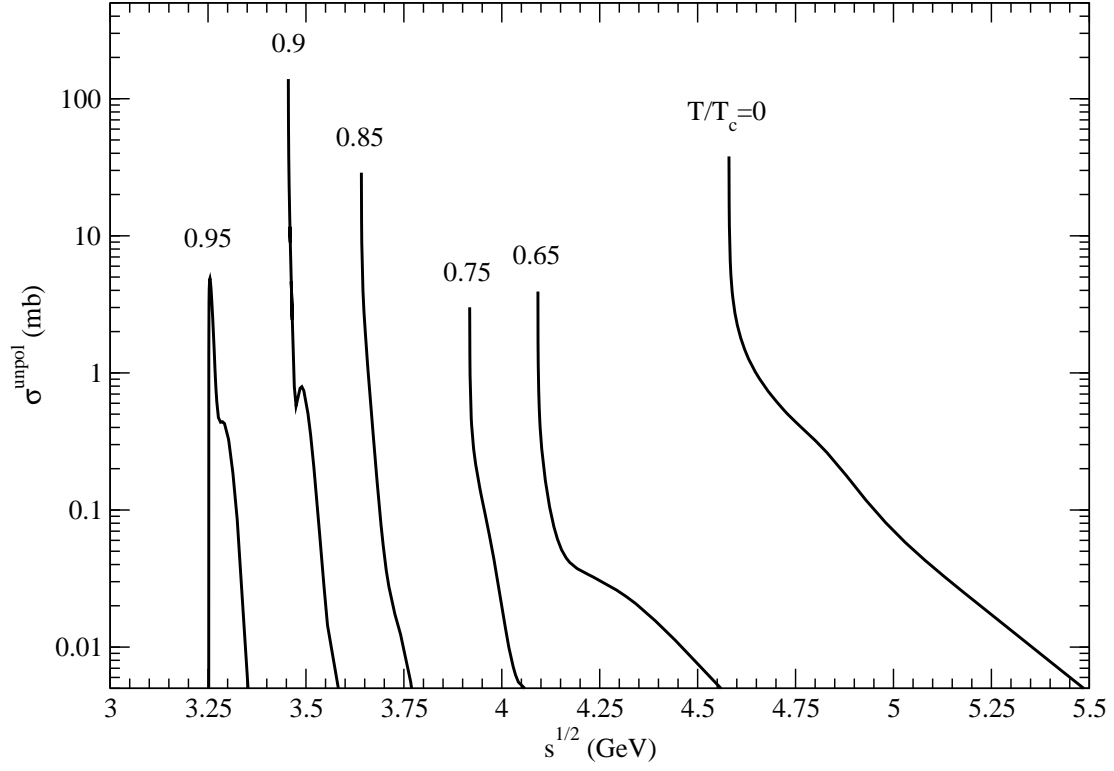


Figure 8: Cross sections for  $K^* + \psi' \rightarrow \bar{D}^* + D_s^+$  at various temperatures.

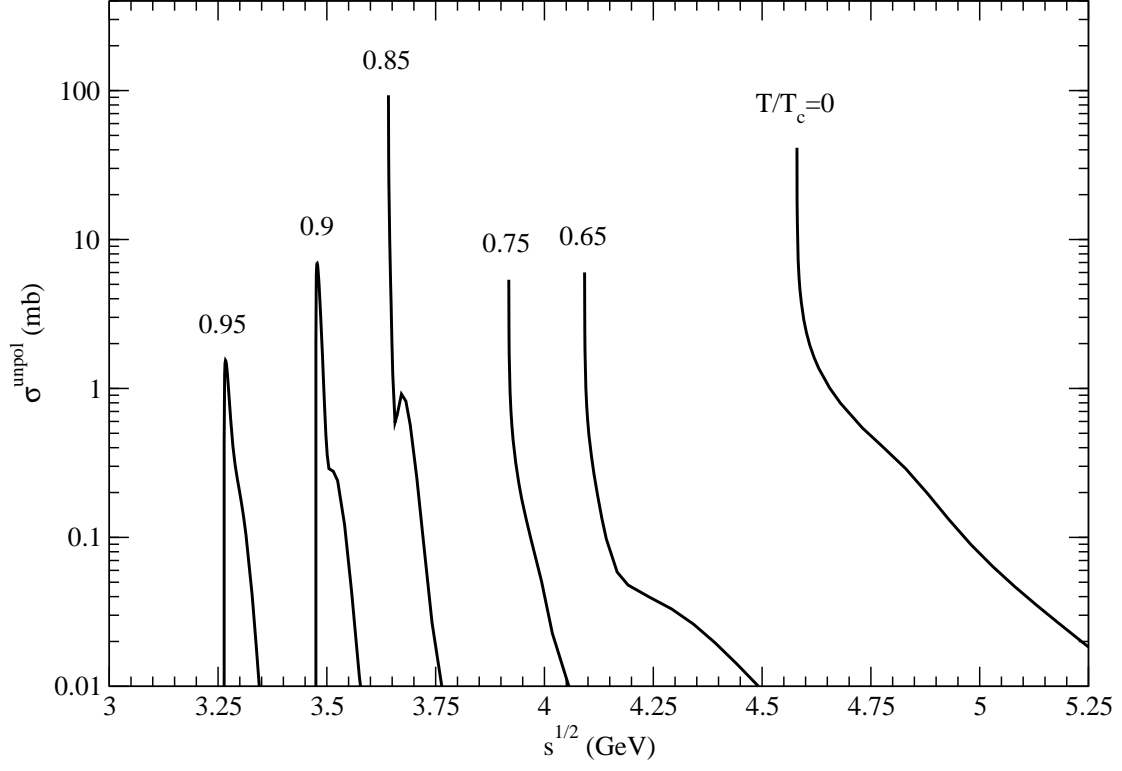


Figure 9: Cross sections for  $K^* + \psi' \rightarrow \bar{D} + D_s^{*+}$  at various temperatures.

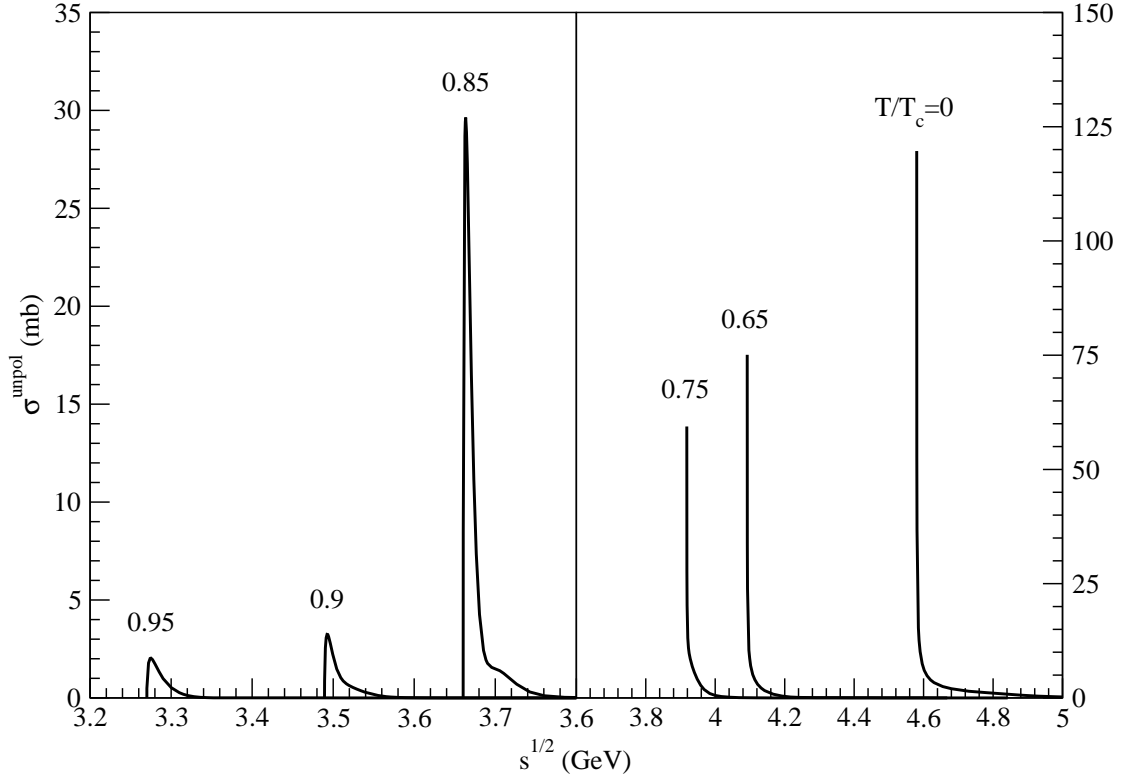


Figure 10: Cross sections for  $K^* + \psi' \rightarrow \bar{D}^* + D_s^{*+}$  at various temperatures.

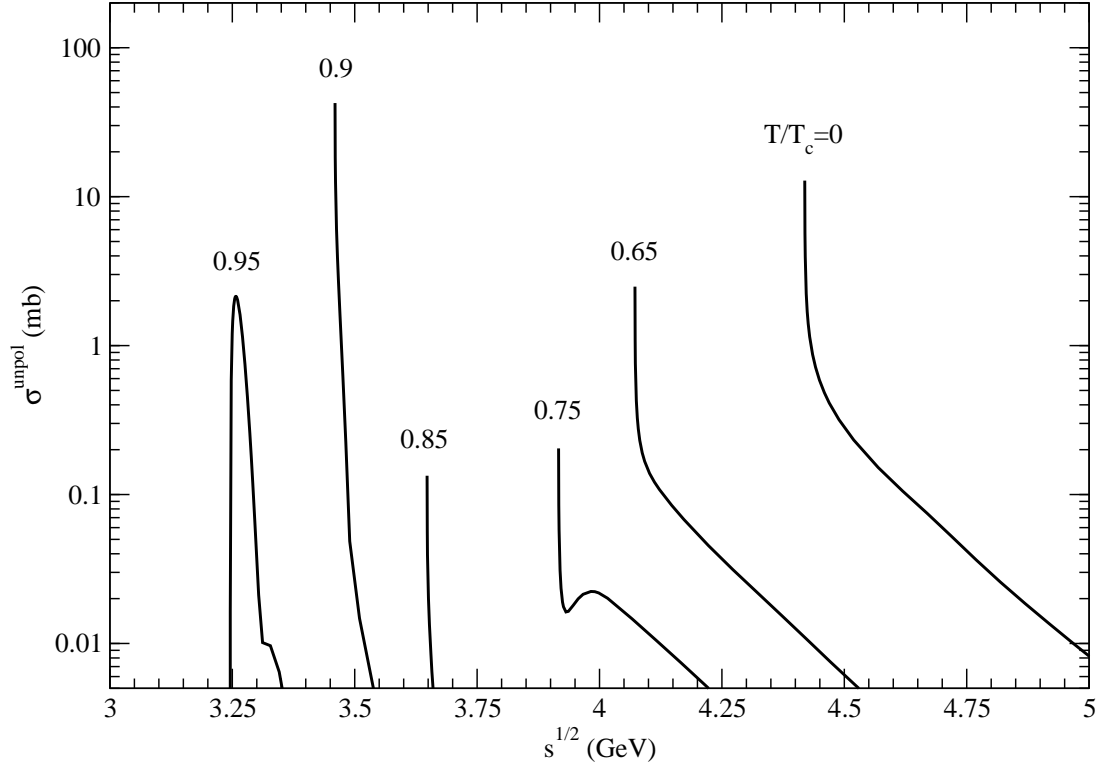


Figure 11: Cross sections for  $K^* + \chi_c \rightarrow \bar{D} + D_s^+$  at various temperatures.

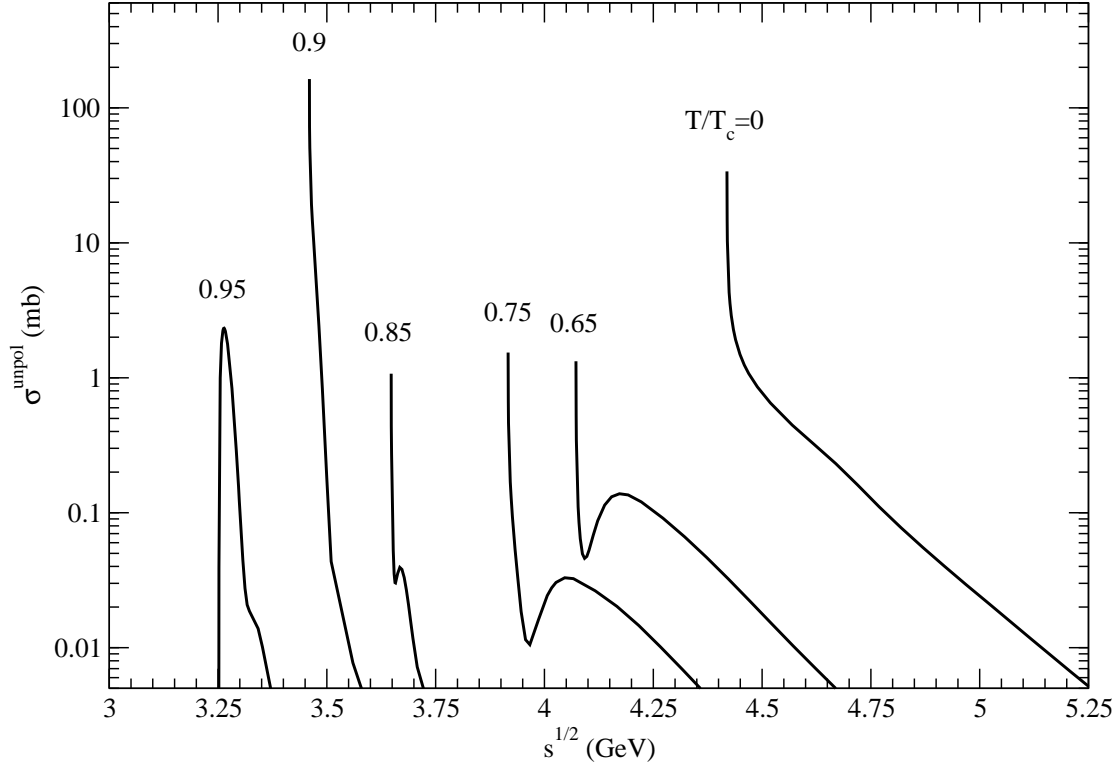


Figure 12: Cross sections for  $K^* + \chi_c \rightarrow \bar{D}^* + D_s^+$  at various temperatures.

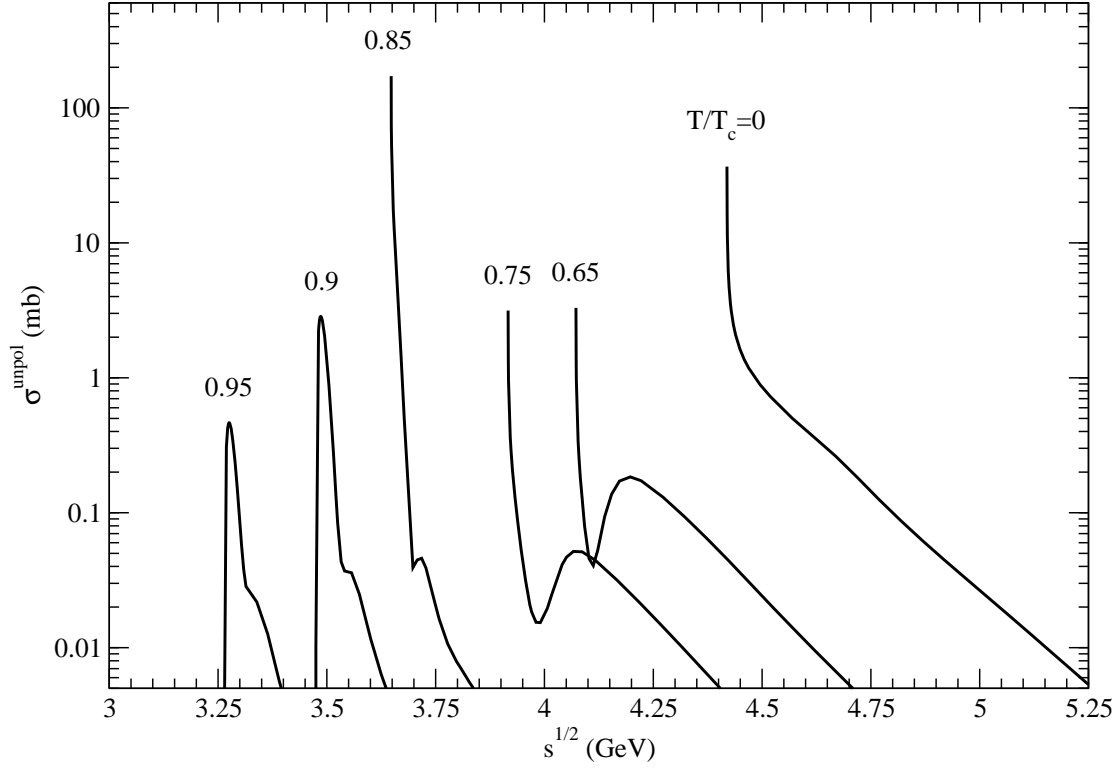


Figure 13: Cross sections for  $K^* + \chi_c \rightarrow \bar{D} + D_s^{*+}$  at various temperatures.

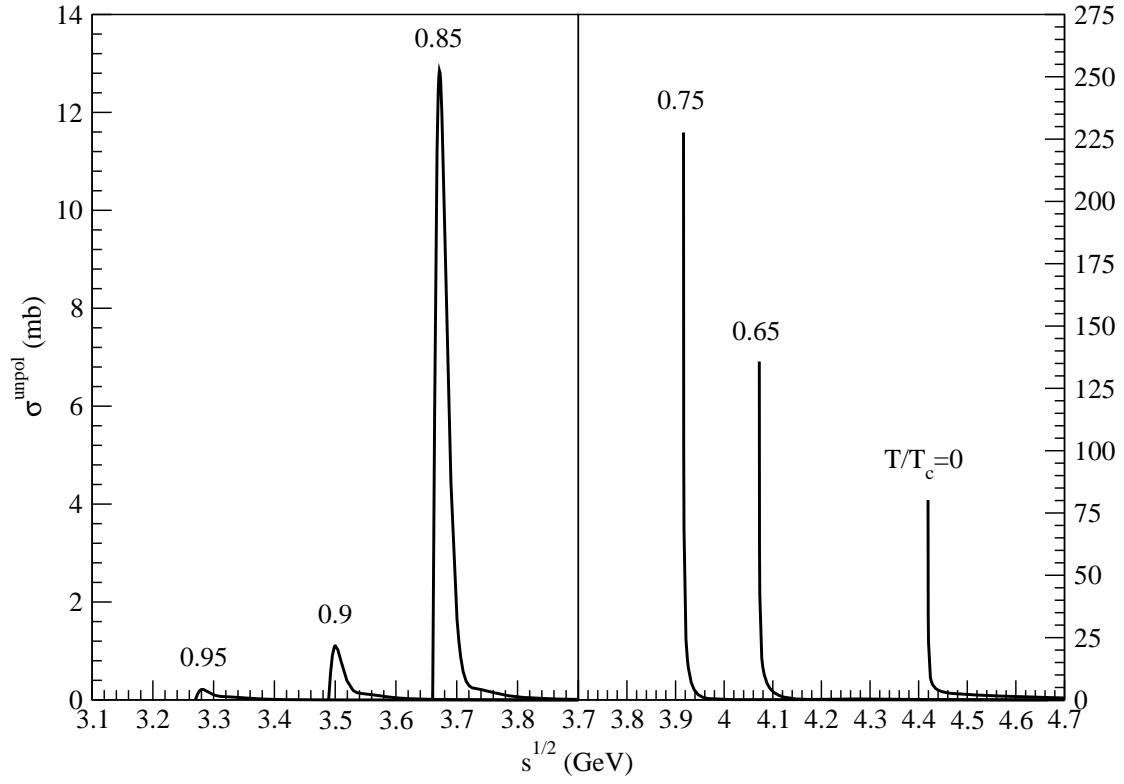


Figure 14: Cross sections for  $K^* + \chi_c \rightarrow \bar{D}^* + D_s^{*+}$  at various temperatures.

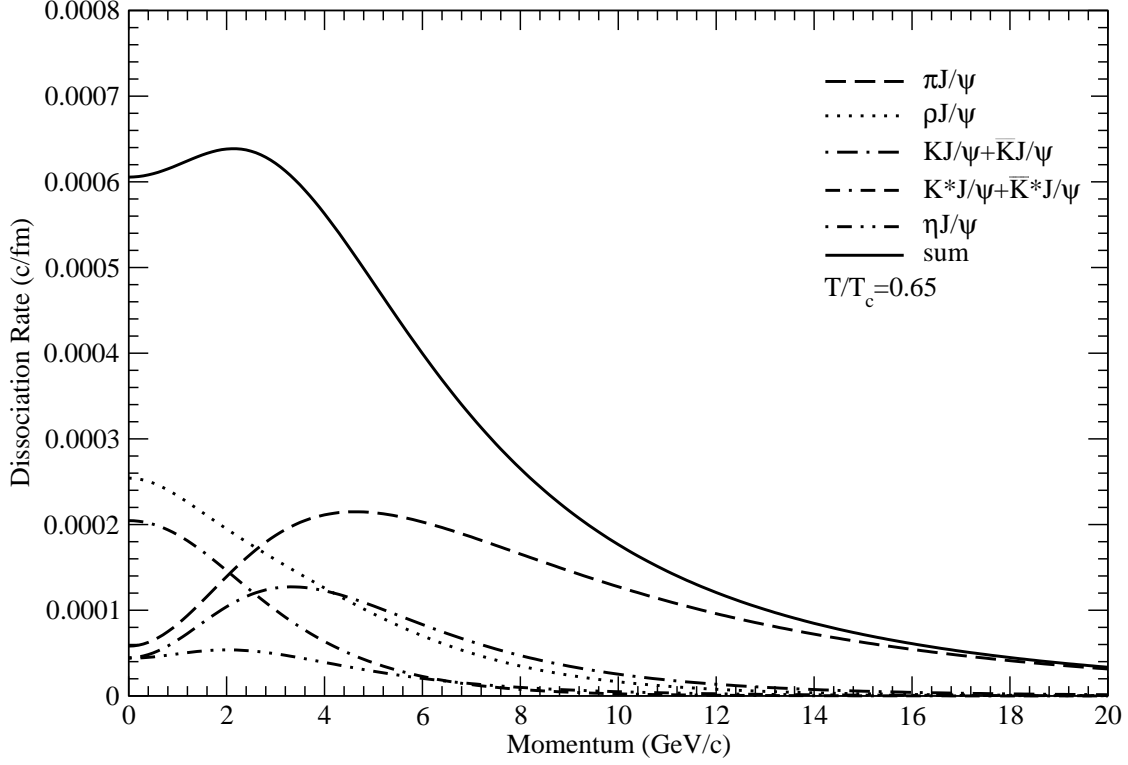


Figure 15: Versus the  $J/\psi$  momentum the dissociation rate of  $J/\psi$  with  $\pi$  (dashed curve), the one of  $J/\psi$  with  $\rho$  (dotted curve), the sum (dot-dashed curve) of the ones of  $J/\psi$  with  $K$  and with  $\bar{K}$ , the sum (dot-dash-dashed curve) of the ones of  $J/\psi$  with  $K^*$  and with  $\bar{K}^*$ , and the one of  $J/\psi$  with  $\eta$  (dot-dot-dashed curve) at  $T = 0.65T_c$ . The solid curve represents the sum of these dissociation rates.

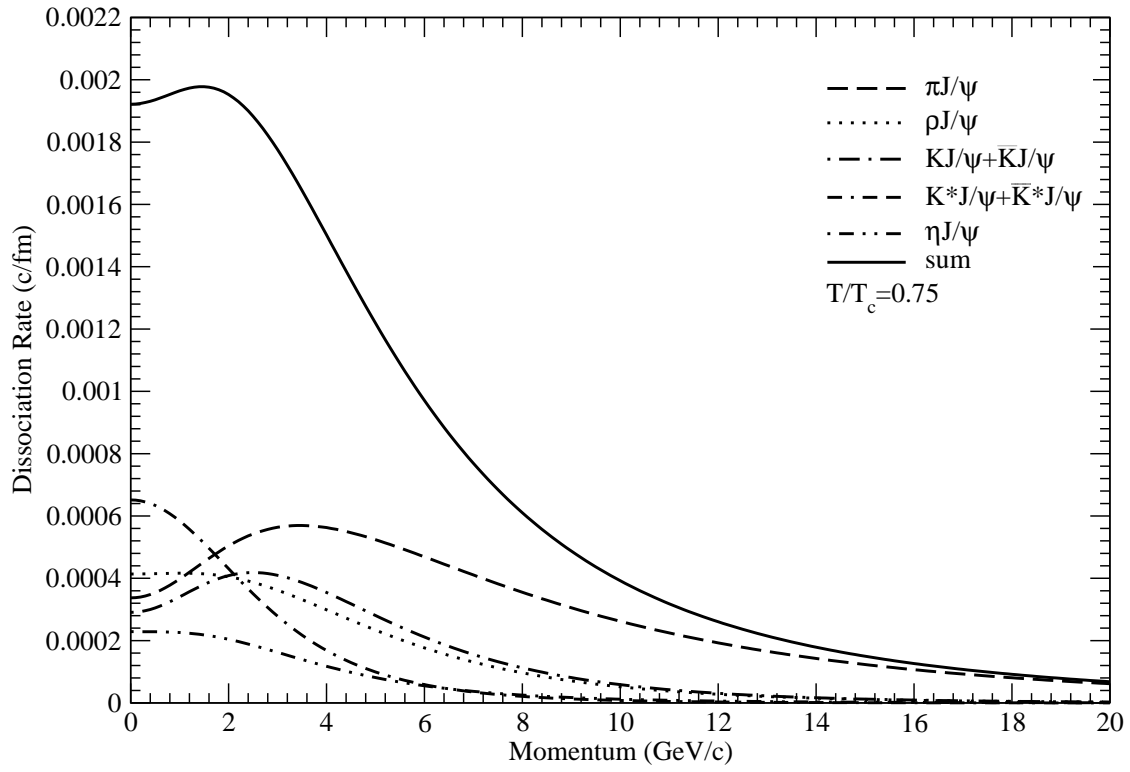


Figure 16: The same as Fig. 15 except for the temperature  $0.75T_c$  .

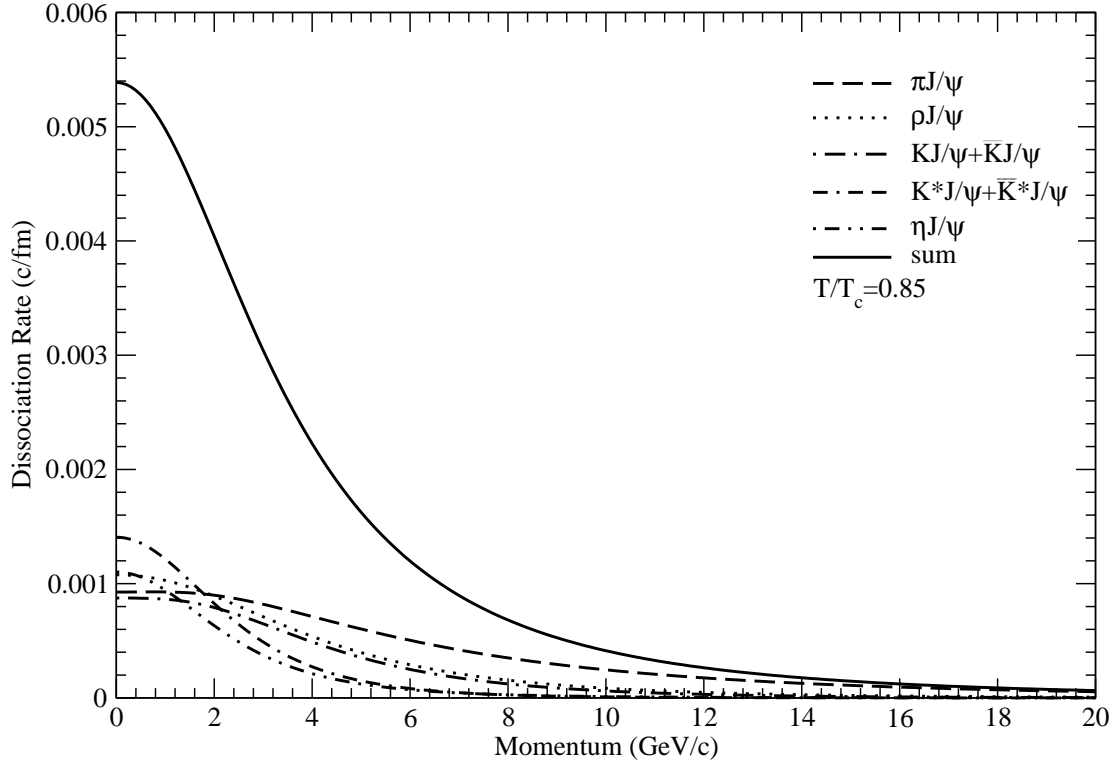


Figure 17: The same as Fig. 15 except for the temperature  $0.85T_c$  .

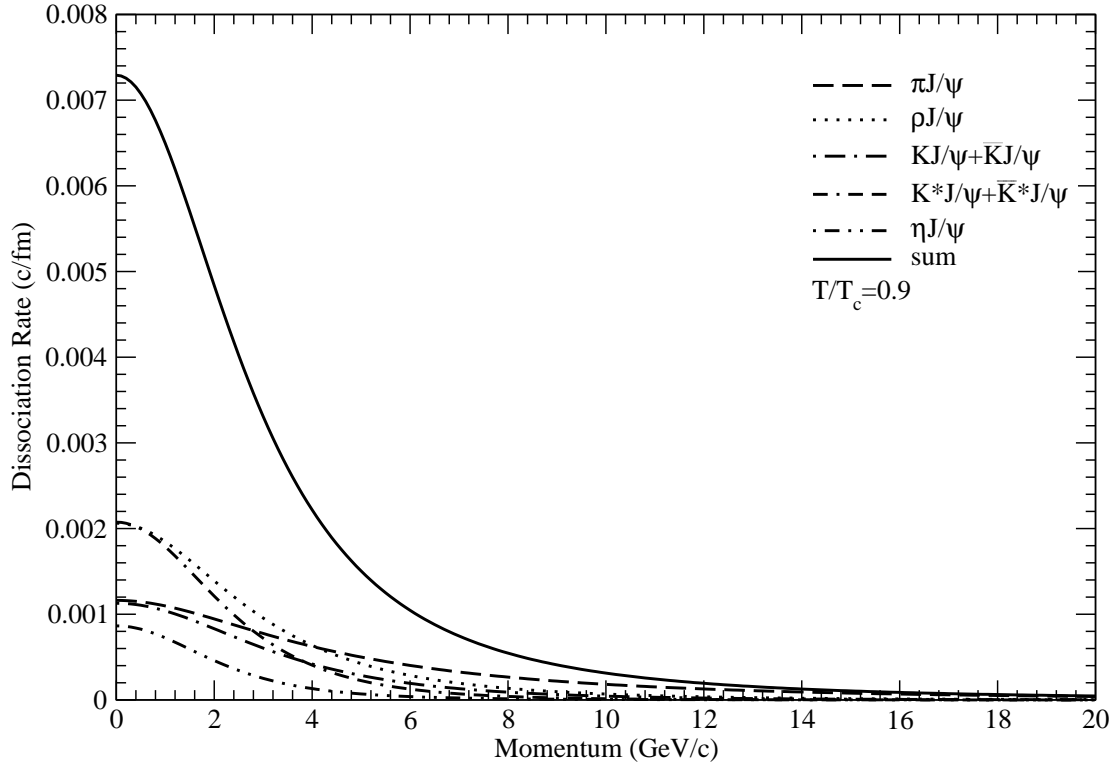


Figure 18: The same as Fig. 15 except for the temperature  $0.9T_c$ .

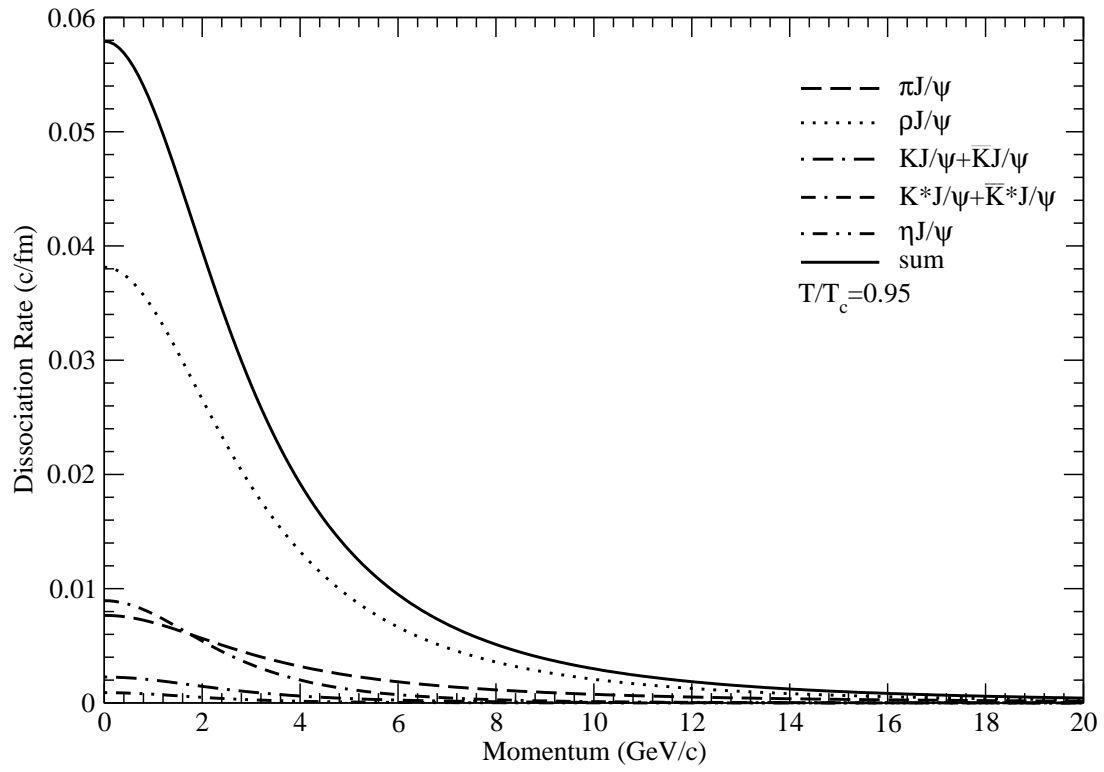


Figure 19: The same as Fig. 15 except for the temperature  $0.95T_c$  .

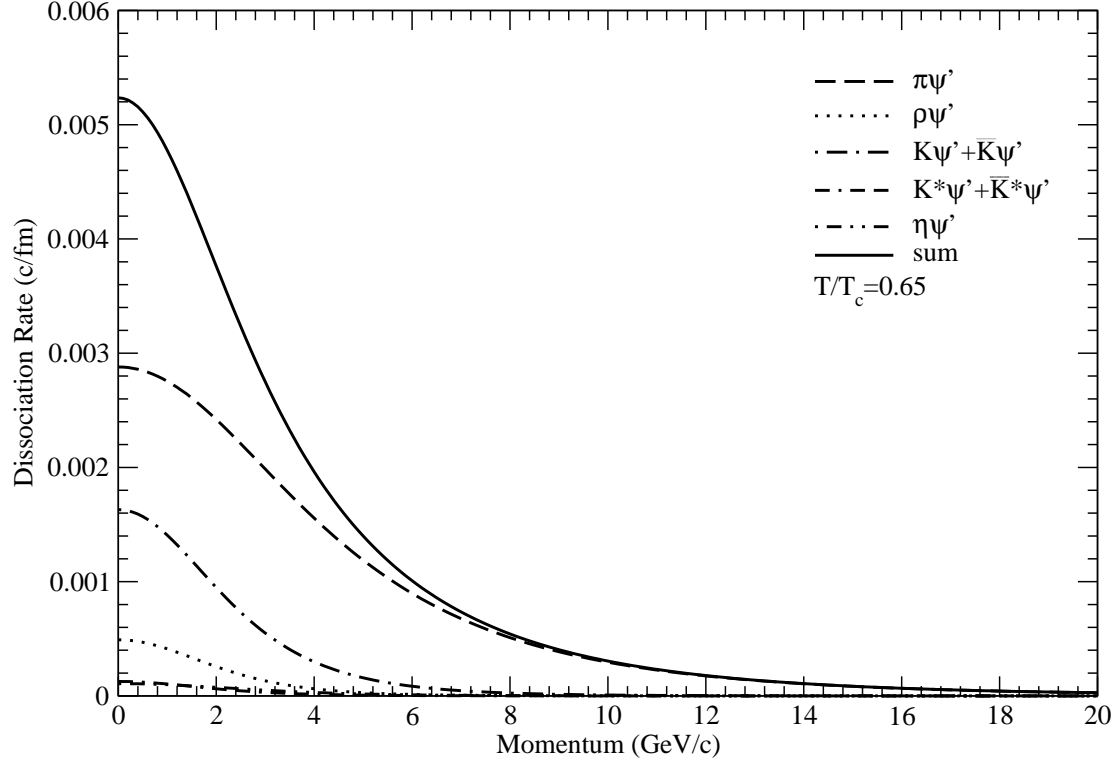


Figure 20: Versus the  $\psi'$  momentum the dissociation rate of  $\psi'$  with  $\pi$  (dashed curve), the one of  $\psi'$  with  $\rho$  (dotted curve), the sum (dot-dashed curve) of the ones of  $\psi'$  with  $K$  and with  $\bar{K}$ , the sum (dot-dash-dashed curve) of the ones of  $\psi'$  with  $K^*$  and with  $\bar{K}^*$ , and the one of  $\psi'$  with  $\eta$  (dot-dot-dashed curve) at  $T = 0.65T_c$ . The solid curve represents the sum of these dissociation rates.

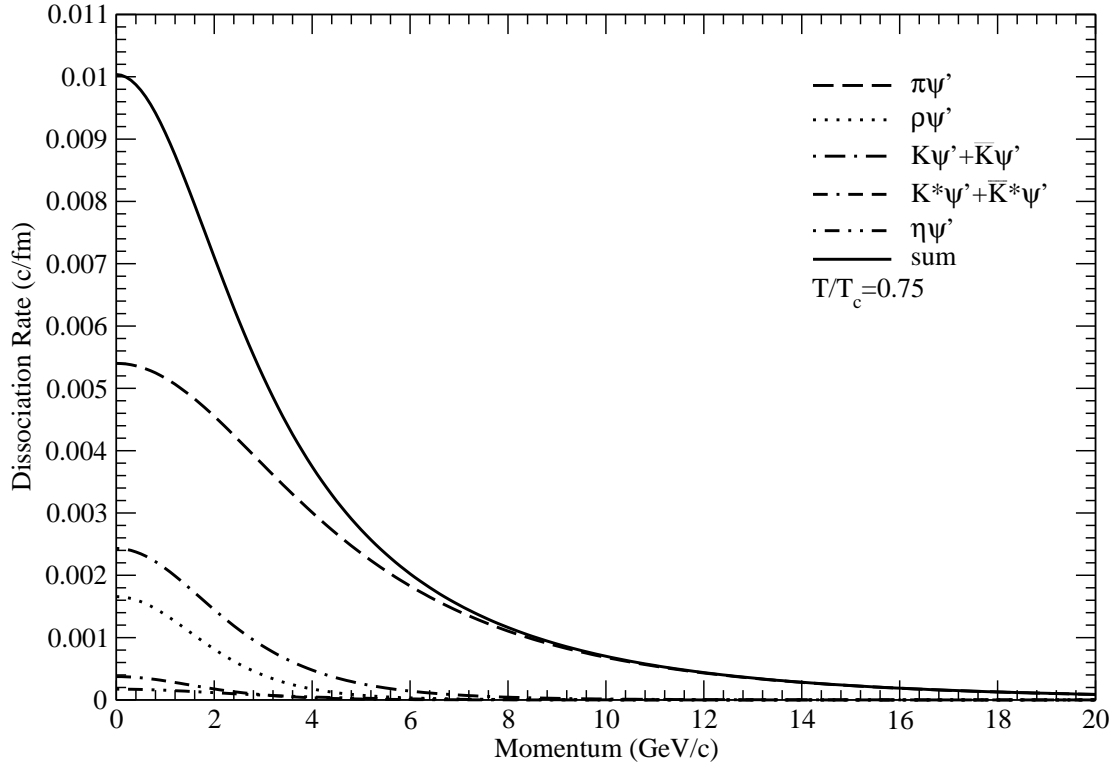


Figure 21: The same as Fig. 20 except for the temperature  $0.75T_c$ .

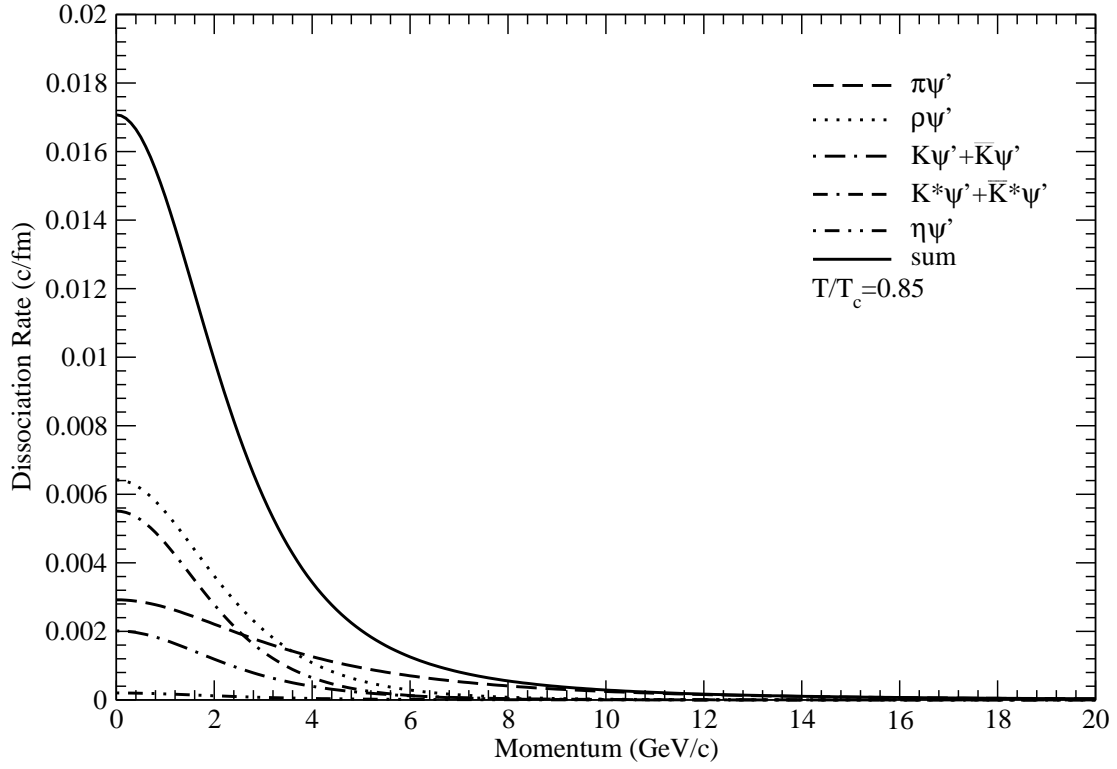


Figure 22: The same as Fig. 20 except for the temperature  $0.85T_c$ .

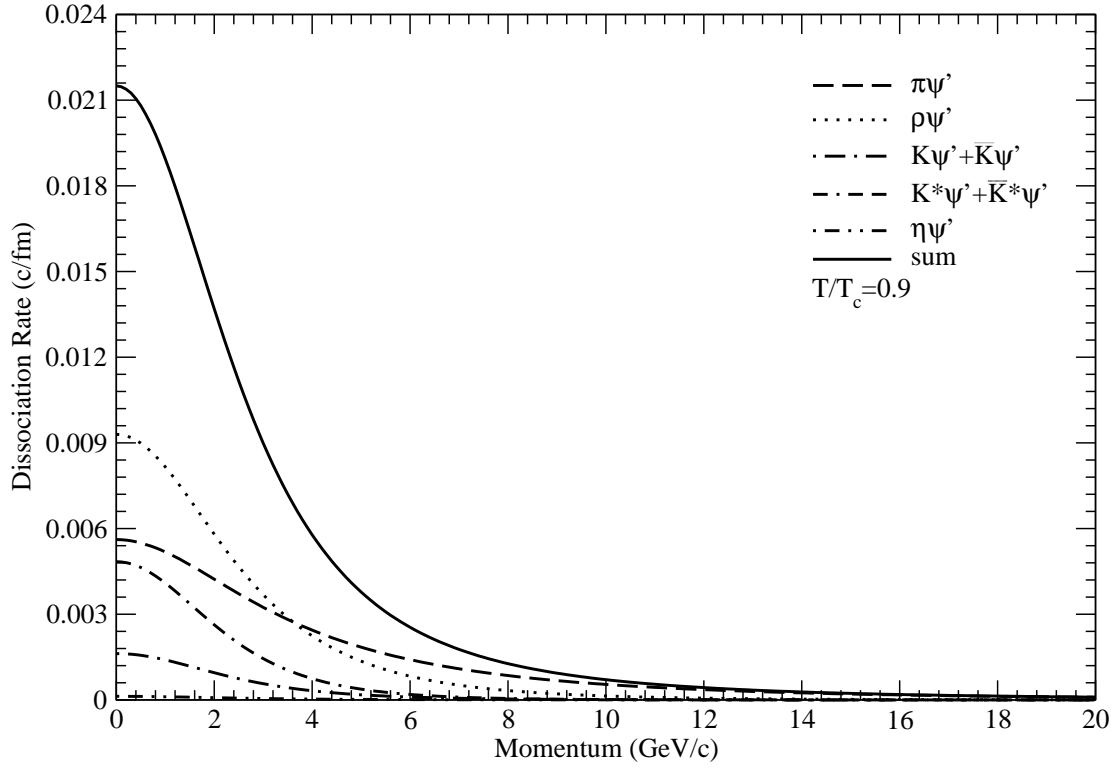


Figure 23: The same as Fig. 20 except for the temperature  $0.9T_c$ .

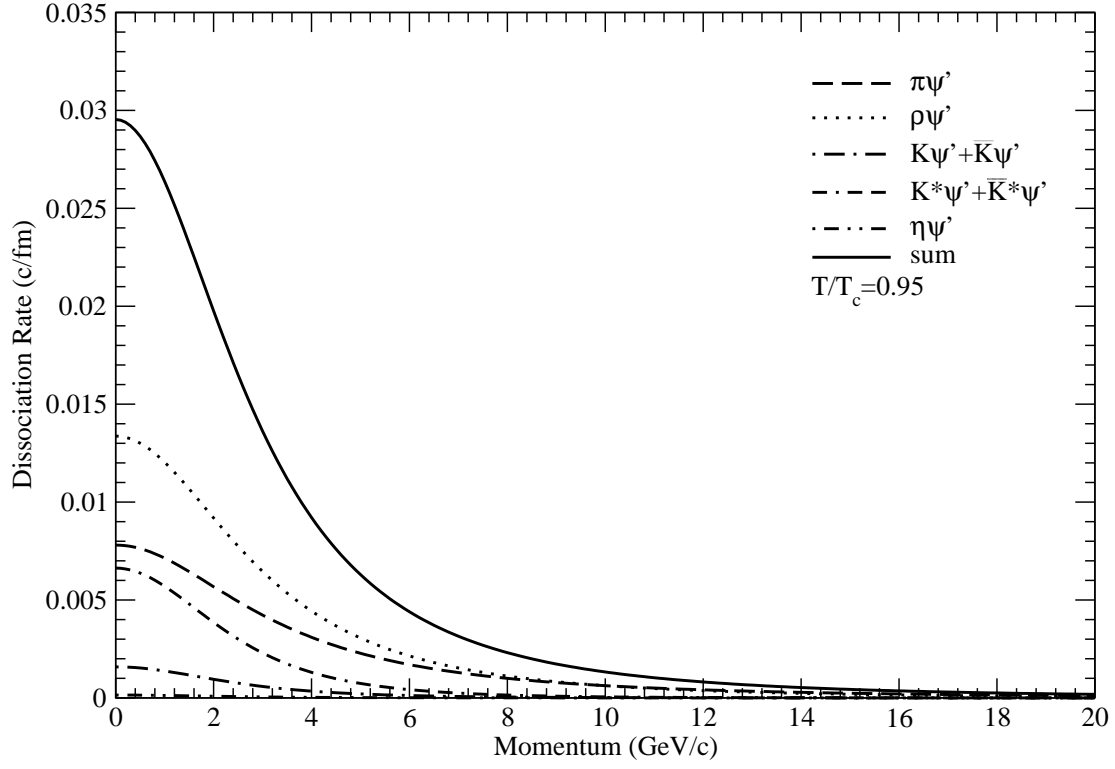


Figure 24: The same as Fig. 20 except for the temperature  $0.95T_c$ .

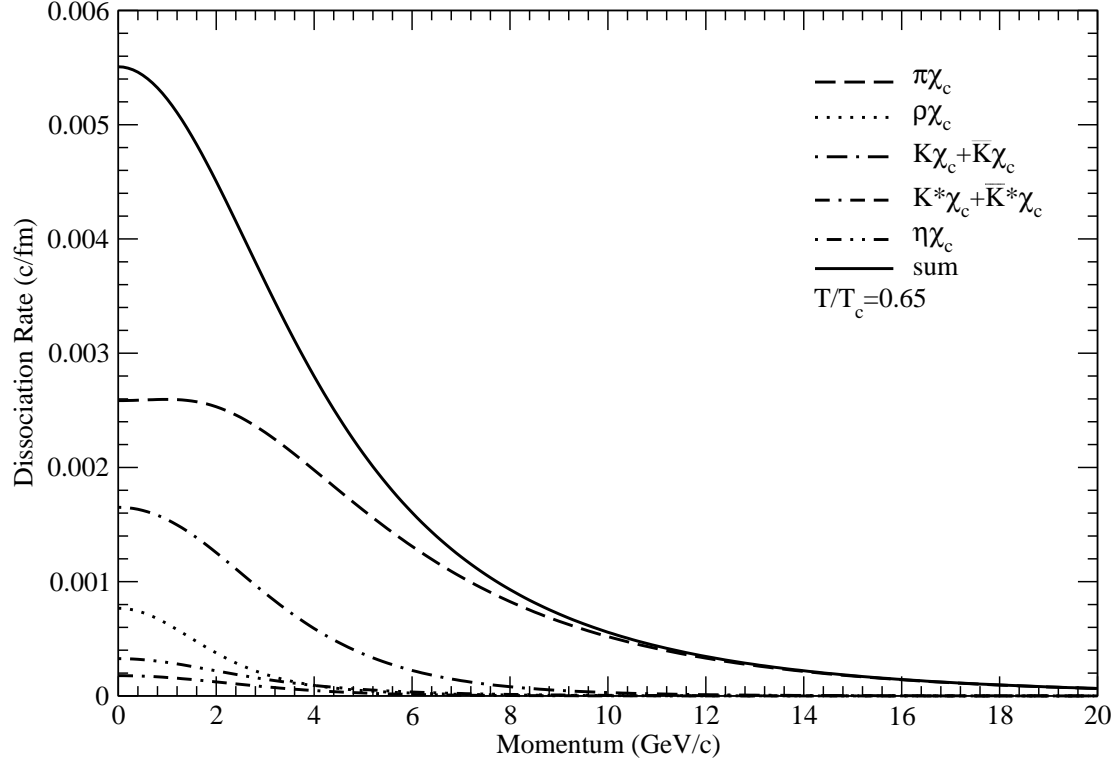


Figure 25: Versus the  $\chi_c$  momentum the dissociation rate of  $\chi_c$  with  $\pi$  (dashed curve), the one of  $\chi_c$  with  $\rho$  (dotted curve), the sum (dot-dashed curve) of the ones of  $\chi_c$  with  $K$  and with  $\bar{K}$ , the sum (dot-dash-dashed curve) of the ones of  $\chi_c$  with  $K^*$  and with  $\bar{K}^*$ , and the one of  $\chi_c$  with  $\eta$  (dot-dot-dashed curve) at  $T = 0.65T_c$ . The solid curve represents the sum of these dissociation rates.

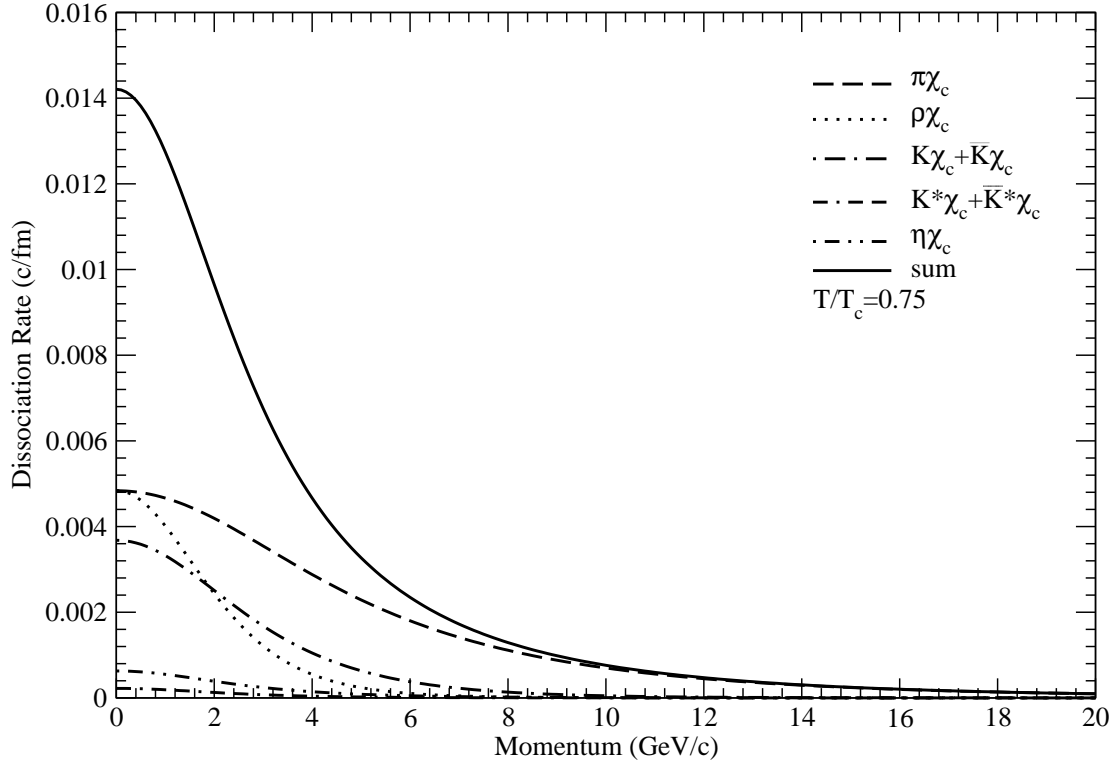


Figure 26: The same as Fig. 25 except for the temperature  $0.75T_c$ .

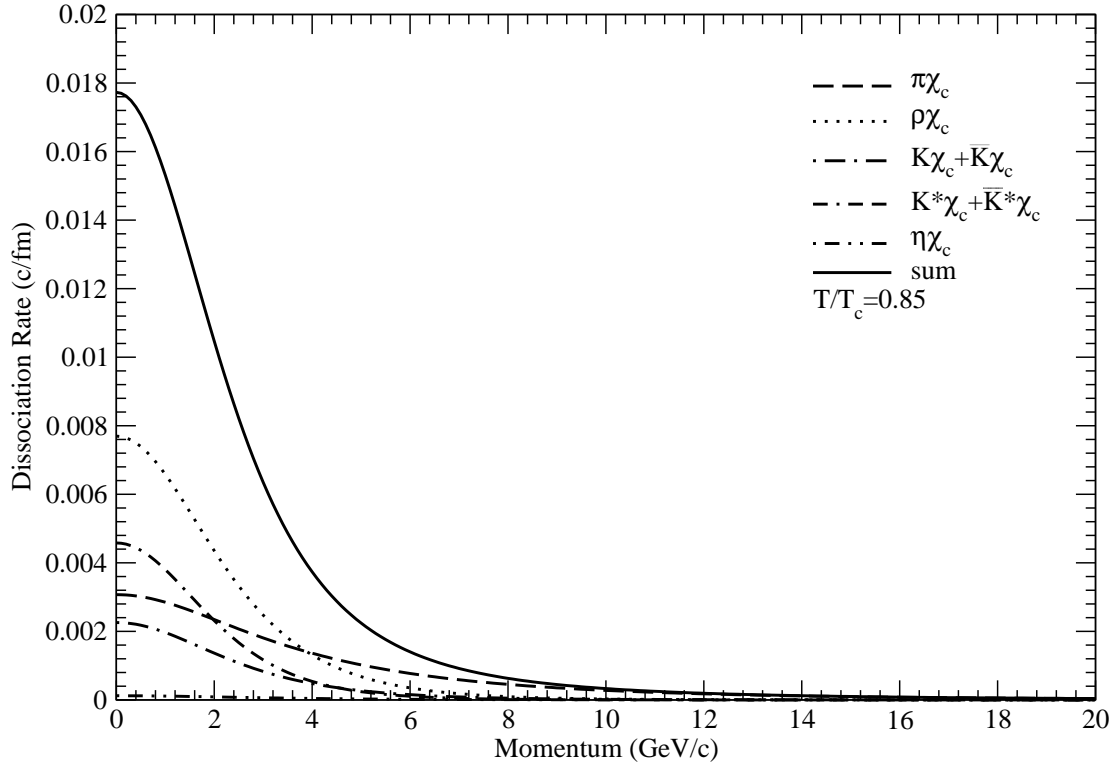


Figure 27: The same as Fig. 25 except for the temperature  $0.85T_c$ .

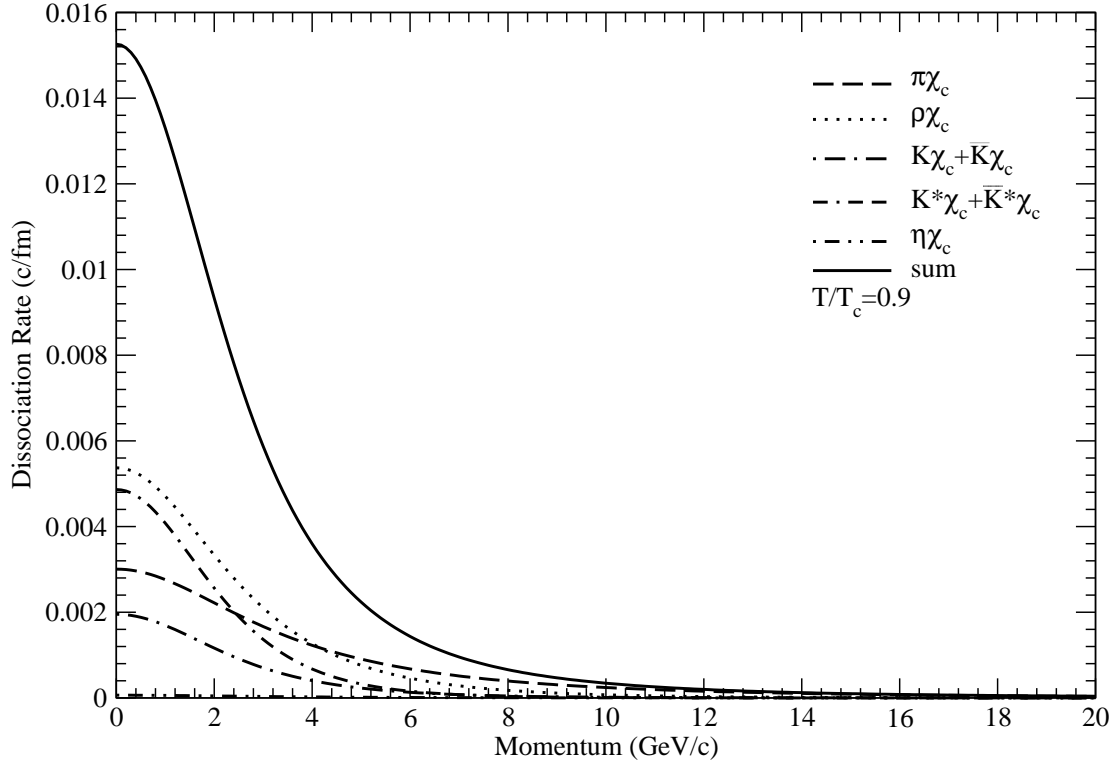


Figure 28: The same as Fig. 25 except for the temperature  $0.9T_c$ .

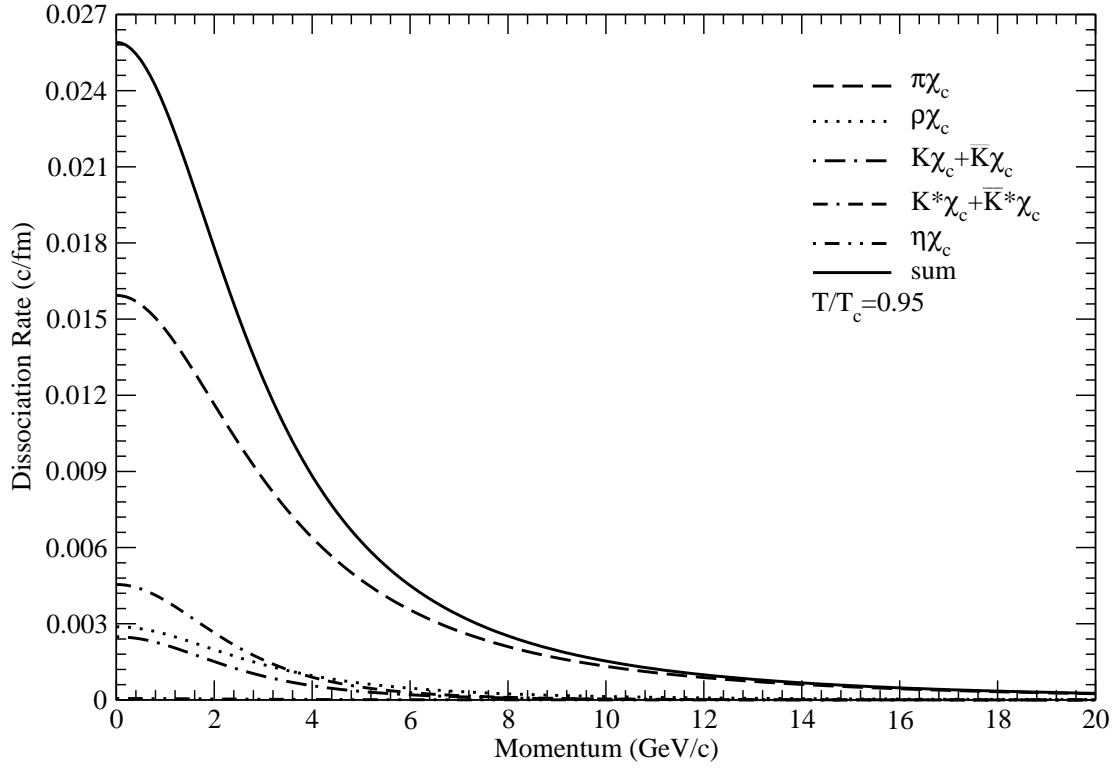


Figure 29: The same as Fig. 25 except for the temperature  $0.95T_c$ .

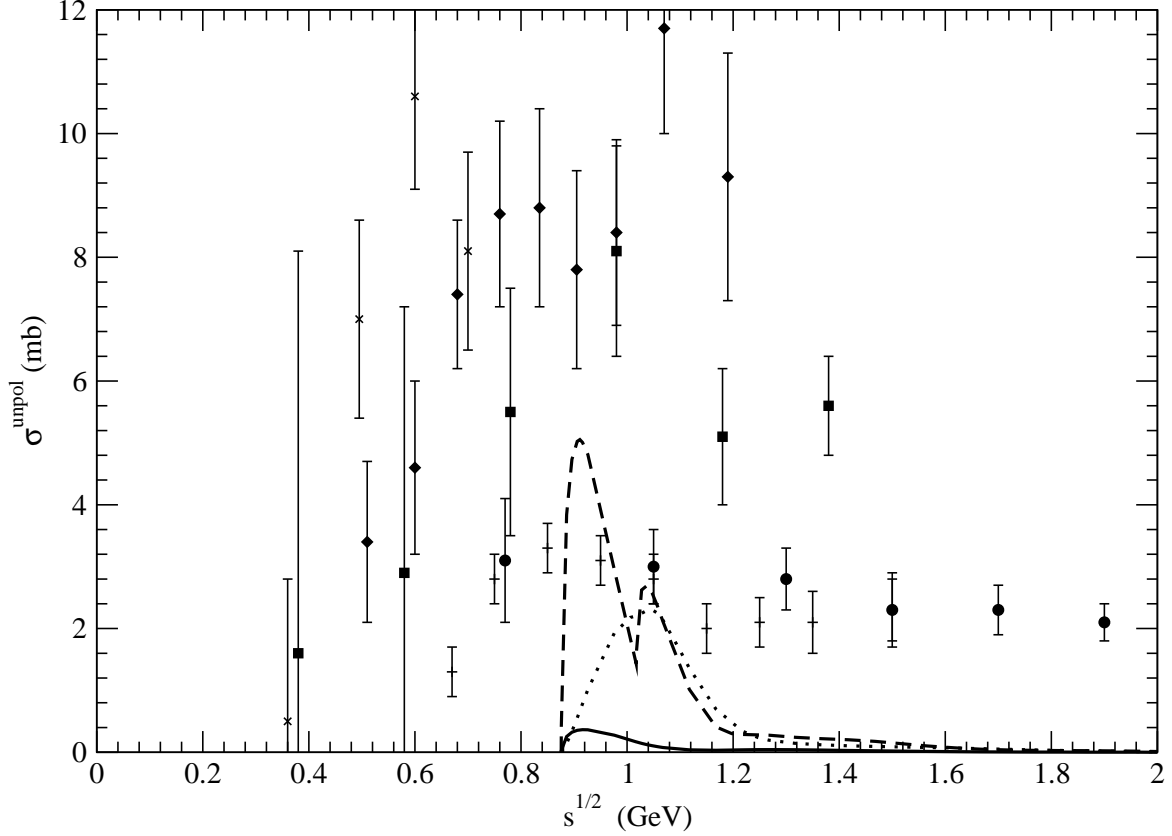


Figure 30: Cross sections for  $\pi$ -induced reactions that are governed by quark interchange. Our theoretical results are shown by the solid, dashed, and dotted curves which stand for unpolarized cross sections for  $\pi J/\psi \rightarrow \bar{D}^*D + \bar{D}D^* + \bar{D}^*D^*$ , for  $\pi\psi' \rightarrow \bar{D}^*D + \bar{D}D^* + \bar{D}^*D^*$ , and for  $\pi\chi_c \rightarrow \bar{D}^*D + \bar{D}D^* + \bar{D}^*D^*$ , respectively. The curves translate by  $-3$  GeV in  $\sqrt{s}$ . Experimental data of elastic  $\pi^-\pi^-$  cross section:  $\times$ , Ref. [34];  $\square$ , Ref. [41];  $\diamond$ , Ref. [37]. Experimental data of elastic  $\pi^-K^-$  cross section:  $+$ , Ref. [42];  $\circ$ , Ref. [43].

Table 1: Quantities relevant to the cross sections for the  $K^*J/\psi$  dissociation reactions.  $a_1$  and  $a_2$  are in units of millibarns;  $b_1$ ,  $b_2$ ,  $d_0$ , and  $\sqrt{s_z}$  are in units of GeV;  $c_1$  and  $c_2$  are dimensionless.

Reactions	$T/T_c$	$a_1$	$b_1$	$c_1$	$a_2$	$b_2$	$c_2$	$d_0$	$\sqrt{s_z}$
$K^*J/\psi \rightarrow \bar{D}D_s^+$	0	0.0466	0.021	0.51	0.0587	0.26	5.26	0.25	4.88
	0.65	0.145	0.02	0.51	0.039	0.04	1.72	0.03	4.59
	0.75	0.13	0.008	0.50	0.16	0.039	1.23	0.022	4.37
	0.85	0.21	0.009	0.46	0.33	0.021	0.56	0.015	3.73
	0.9	0.04	0.008	0.82	0.42	0.013	0.48	0.012	3.59
	0.95	0.23	0.007	0.59	0.52	0.010	0.46	0.0081	3.37
$K^*J/\psi \rightarrow \bar{D}^*D_s^+$	0	0.407	0.024	0.59	0.162	0.288	44.8	0.03	4.98
	0.65	1.016	0.017	0.494	0.205	0.033	0.79	0.02	4.47
	0.75	0.860	0.017	0.52	0.026	0.023	0.48	0.017	3.92
	0.85	0.355	0.006	0.49	0.333	0.025	1.29	0.015	3.71
	0.9	0.36	0.007	0.44	0.29	0.017	0.78	0.01	3.57
	0.95	0.74	0.006	0.45	0.49	0.013	0.71	0.0081	3.36
$K^*J/\psi \rightarrow \bar{D}D_s^{*+}$	0	0.486	0.0228	0.560	0.231	0.270	52.4	0.02	4.84
	0.65	0.539	0.0186	0.53	0.127	0.27	31.5	0.02	4.63
	0.75	0.18	0.017	0.45	0.13	0.019	0.65	0.017	4.51
	0.85	0.055	0.010	0.51	0.038	0.017	0.49	0.012	4.26
	0.9	0.043	0.005	0.52	0.065	0.009	0.50	0.0071	3.87
	0.95	0.39	0.004	0.41	0.52	0.009	0.68	0.0071	3.35
$K^*J/\psi \rightarrow \bar{D}^*D_s^{*+}$	0	0.743	0.022	0.54	0.458	0.26	5.78	0.025	5.04
	0.65	0.327	0.018	0.49	0.180	0.228	5.03	0.018	4.77
	0.75	0.199	0.0149	0.49	0.081	0.225	4.78	0.015	4.61
	0.85	0.0430	0.0097	0.50	0.0129	0.1648	3.05	0.01	4.28
	0.9	0.040	0.003	0.43	0.029	0.008	0.90	0.0046	3.93
	0.95	1.39	0.003	0.45	1.33	0.011	1.13	0.0061	3.34

Table 2: The same as Table 1 except for the  $K^*\psi'$  dissociation.

Reactions	$T/T_c$	$a_1$	$b_1$	$c_1$	$a_2$	$b_2$	$c_2$	$d_0$	$\sqrt{s_z}$
$K^*\psi' \rightarrow \bar{D}D_s^+$	0	0.012	0.06	0.41	0.017	0.11	0.70	0.1	5.5
	0.65	0.0030	0.08	0.44	0.0006	0.17	2.27	0.1	4.98
	0.75	0.00063	0.010	0.51	0.00101	0.168	1.44	0.15	4.81
	0.85	0.0025	0.006	0.58	0.0021	0.023	0.39	0.007	4.22
	0.9	0.022	0.018	0.389	0.099	0.025	3.558	0.022	3.58
	0.95	2.91	0.001	0.52	3.20	0.005	1.52	0.0026	3.33
$K^*\psi' \rightarrow \bar{D}^*D_s^+$	0	0.040	0.03	0.47	0.057	0.16	1.44	0.1	5.74
	0.65	0.0061	0.015	0.48	0.0071	0.182	1.89	0.168	5.13
	0.75	0.0059	0.010	0.53	0.0066	0.039	2.09	0.026	4.71
	0.85	0.080	0.007	0.44	0.041	0.010	1.04	0.0092	3.78
	0.9	0.75	0.001	0.45	0.76	0.004	1.15	0.002	3.54
	0.95	3.32	0.002	0.46	1.87	0.005	0.92	0.0031	3.34
$K^*\psi' \rightarrow \bar{D}D_s^{*+}$	0	0.066	0.07	0.47	0.024	0.19	2.11	0.1	5.49
	0.65	0.01349	0.018	0.51	0.00949	0.201	2.56	0.022	4.94
	0.75	0.0158	0.018	0.48	0.0038	0.040	1.49	0.023	4.67
	0.85	0.637	0.0020	0.49	0.279	0.036	5.28	0.003	3.77
	0.9	4.15	0.0024	0.38	2.91	0.0036	0.93	0.0031	3.55
	0.95	0.93	0.0033	0.78	0.64	0.0040	0.27	0.0031	3.34
$K^*\psi' \rightarrow \bar{D}^*D_s^{*+}$	0	0.179	0.03	0.502	0.214	0.19	2.523	0.15	5.48
	0.65	0.150	0.019	0.44	0.225	0.023	0.62	0.022	4.67
	0.75	0.50	0.017	0.53	0.35	0.022	1.79	0.022	4.11
	0.85	17.96	0.002	0.43	13.51	0.005	0.89	0.0031	3.74
	0.9	2.06	0.003	0.65	1.28	0.006	0.33	0.0031	3.58
	0.95	1.28	0.003	0.45	0.98	0.010	0.82	0.0051	3.34

Table 3: The same as Table 1 except for the  $K^*\chi_c$  dissociation.

Reactions	$T/T_c$	$a_1$	$b_1$	$c_1$	$a_2$	$b_2$	$c_2$	$d_0$	$\sqrt{s_z}$
$K^*\chi_c \rightarrow \bar{D}D_s^+$	0	0.001345	0.218	5.57	0.02402	0.0801	0.484	0.1	5.31
	0.65	0.00377	0.0314	0.454	0.0074	0.1381	1.232	0.1	4.93
	0.75	0.00013	0.004	0.39	0.0032	0.14	1.5	0.1	4.78
	0.85	0.00025	0.0058	0.44	0.0003	0.13	1.67	0.15	4.46
	0.9	0.1	0.0011	0.47	0.18	0.0063	1.22	0.005	3.54
	0.95	1.52	0.014	2.2	0.81	0.007	1.2	0.011	3.3
$K^*\chi_c \rightarrow \bar{D}^*D_s^+$	0	0.013	0.194	4.03	0.077	0.079	0.473	0.1	5.3
	0.65	0.00116	0.0047	0.47	0.029	0.168	2.3	0.15	4.91
	0.75	0.0028	0.007	0.57	0.0088	0.195	3.29	0.15	4.74
	0.85	0.00173	0.0017	0.51	0.00441	0.028	2.9	0.025	4.19
	0.9	1.23	0.003	0.5	0.79	0.01	1.6	0.005	3.51
	0.95	0.77	0.008	0.88	1.65	0.013	2.05	0.012	3.32
$K^*\chi_c \rightarrow \bar{D}D_s^{*+}$	0	0.0178	0.188	3.69	0.0844	0.079	0.473	0.1	5.29
	0.65	0.0051	0.0069	0.56	0.048	0.176	3.62	0.15	4.9
	0.75	0.0074	0.01	0.53	0.0162	0.197	5.1	0.15	4.74
	0.85	0.5	0.0103	1.83	1.13	0.003	0.52	0.005	3.7
	0.9	1.57	0.012	1.89	1.32	0.01	1.38	0.011	3.57
	0.95	0.05	0.003	1.52	0.46	0.012	1.88	0.012	3.4
$K^*\chi_c \rightarrow \bar{D}^*D_s^{*+}$	0	0.155	0.0306	0.45	0.319	0.178	2.11	0.15	5.27
	0.65	0.56	0.0117	0.5	0.163	0.22	7.58	0.01	4.76
	0.75	0.6	0.0038	0.44	0.6	0.011	0.78	0.008	4.37
	0.85	4.3	0.009	0.9	8.8	0.012	1.9	0.011	3.77
	0.9	0.84	0.012	1.74	0.29	0.007	0.65	0.011	3.66
	0.95	0.079	0.023	0.5	0.151	0.01	2	0.011	3.47

Table 4: Reactions that contribute to the dissociation rate of charmonium and meson.  $\sigma^{\text{unpol}}$  in Eqs. (30) and (31) is the sum of the unpolarized cross sections for the reactions listed in each row of the third column.

charmonium	meson	reactions
$J/\psi$	$\pi$	$\pi J/\psi \rightarrow \bar{D}^* D, \bar{D} D^*, \bar{D}^* D^*$
$J/\psi$	$\rho$	$\rho J/\psi \rightarrow \bar{D} D, \bar{D}^* D, \bar{D} D^*, \bar{D}^* D^*$
$J/\psi$	$K$	$K J/\psi \rightarrow \bar{D}^* D_s^+, \bar{D} D_s^{*+}, \bar{D}^* D_s^{*+}$
$J/\psi$	$\bar{K}$	$\bar{K} J/\psi \rightarrow D_s^{*-} D, D_s^- D^*, D_s^{*-} D^*$
$J/\psi$	$K^*$	$K^* J/\psi \rightarrow \bar{D} D_s^+, \bar{D}^* D_s^+, \bar{D} D_s^{*+}, \bar{D}^* D_s^{*+}$
$J/\psi$	$\bar{K}^*$	$\bar{K}^* J/\psi \rightarrow D_s^- D, D_s^{*-} D, D_s^- D^*, D_s^{*-} D^*$
$J/\psi$	$\eta$	$\eta J/\psi \rightarrow \bar{D}^* D, \bar{D} D^*, \bar{D}^* D^*, D_s^{*-} D_s^+, D_s^- D_s^{*+}, D_s^{*-} D_s^{*+}$
$\psi'$	$\pi$	$\pi \psi' \rightarrow \bar{D}^* D, \bar{D} D^*, \bar{D}^* D^*$
$\psi'$	$\rho$	$\rho \psi' \rightarrow \bar{D} D, \bar{D}^* D, \bar{D} D^*, \bar{D}^* D^*$
$\psi'$	$K$	$K \psi' \rightarrow \bar{D}^* D_s^+, \bar{D} D_s^{*+}, \bar{D}^* D_s^{*+}$
$\psi'$	$\bar{K}$	$\bar{K} \psi' \rightarrow D_s^{*-} D, D_s^- D^*, D_s^{*-} D^*$
$\psi'$	$K^*$	$K^* \psi' \rightarrow \bar{D} D_s^+, \bar{D}^* D_s^+, \bar{D} D_s^{*+}, \bar{D}^* D_s^{*+}$
$\psi'$	$\bar{K}^*$	$\bar{K}^* \psi' \rightarrow D_s^- D, D_s^{*-} D, D_s^- D^*, D_s^{*-} D^*$
$\psi'$	$\eta$	$\eta \psi' \rightarrow \bar{D}^* D, \bar{D} D^*, \bar{D}^* D^*, D_s^{*-} D_s^+, D_s^- D_s^{*+}, D_s^{*-} D_s^{*+}$
$\chi_c$	$\pi$	$\pi \chi_c \rightarrow \bar{D}^* D, \bar{D} D^*, \bar{D}^* D^*$
$\chi_c$	$\rho$	$\rho \chi_c \rightarrow \bar{D} D, \bar{D}^* D, \bar{D} D^*, \bar{D}^* D^*$
$\chi_c$	$K$	$K \chi_c \rightarrow \bar{D}^* D_s^+, \bar{D} D_s^{*+}, \bar{D}^* D_s^{*+}$
$\chi_c$	$\bar{K}$	$\bar{K} \chi_c \rightarrow D_s^{*-} D, D_s^- D^*, D_s^{*-} D^*$
$\chi_c$	$K^*$	$K^* \chi_c \rightarrow \bar{D} D_s^+, \bar{D}^* D_s^+, \bar{D} D_s^{*+}, \bar{D}^* D_s^{*+}$
$\chi_c$	$\bar{K}^*$	$\bar{K}^* \chi_c \rightarrow D_s^- D, D_s^{*-} D, D_s^- D^*, D_s^{*-} D^*$
$\chi_c$	$\eta$	$\eta \chi_c \rightarrow \bar{D}^* D, \bar{D} D^*, \bar{D}^* D^*, D_s^{*-} D_s^+, D_s^- D_s^{*+}, D_s^{*-} D_s^{*+}$